The Dissertation Committee for Christina A. Frederick
certifies that this is the approved version of the following dissertation:

Numerical Methods for Multiscale Inverse Problems

Committee:

Björn Engquist, Supervisor

Todd Arbogast

Omar Ghattas

Kui Ren

Yen-Hsi Tsai

Numerical Methods for Multiscale Inverse Problems

by

Christina A. Frederick, B.S.

DISSERTATION

Presented to the Faculty of the Graduate School of

The University of Texas at Austin

in Partial Fulfillment

of the Requirements

for the Degree of

DOCTOR OF PHILOSOPHY

THE UNIVERSITY OF TEXAS AT AUSTIN

May 2014

Dedicated to my mother.

Acknowledgments

First and foremost, I am deeply grateful for the continuous support, patience, and generosity of my supervisor, Björn Engquist. I am extremely lucky to have a supervisor that cares about my development as an independent researcher. His guidance and warm encouragement has made this a thoughtful and rewarding journey.

I owe a very important debt to Todd Arbogast, Omar Ghattas, Kui Ren, and Richard Tsai for serving as members of my dissertation committee, and am immensely grateful to Kui Ren and Rachel Ward for mentoring me throughout the research process. Special thanks goes to Richard Tsai, I-Liang Chern, Lexing Ying, and Pingbing Ming for supporting my travels to Asia as part of the NSF EAPSI program. I would also like to express my heartfelt appreciation to Marshall Cohen, Kasso Okoudjou, and Jim Yorke for inspiring me to pursue mathematics when I was an undergraduate at the University of Maryland.

Karen Uhlenbeck has been a prominent role model for me during my years at UT, and I have benefited in so many ways from her advocacy for women in mathematics and the outreach programs she generously supports. I cannot express with words my gratitude for all of the help and support I have received from Sandra Catlett, Eva Hernandez, and Dan Knopf.

This work would have not been possible without the generous support from the NSF grants DMS-1217203 and DMS-1317015 and the Texas Consor-

tium for Computational Seismology.

I would like to thank my friends in Austin and elsewhere for being sources of laughter, joy, and support. I am very happy that, in many cases, my friendships with you have extended well beyond our shared time in Austin. Last, but by no means last, I wish to express my heartfelt appreciation to my mother, Magdalena Frederick and my sister Maria Huemmer. Your love and encouragement allowed me to finish this journey, and I hope that this work makes you proud.

Christina Frederick

May 2014

Austin, Texas

Numerical Methods for Multiscale Inverse Problems

Publication No. _____

Christina A. Frederick, Ph.D.
The University of Texas at Austin, 2014

Supervisor: Björn Engquist

This dissertation focuses on inverse problems for partial differential equations with multiscale coefficients in which the goal is to determine the coefficients in the equation using solution data. Such problems pose a huge computational challenge, in particular when the coefficients are of multiscale form. When faced with balancing computational cost with accuracy, most approaches only deal with models of large scale behavior and, for example, account for microscopic processes by using effective or empirical equations of state on the continuum scale to simplify computations. Obtaining these models often results in the loss of the desired fine scale details. In this thesis we introduce ways to overcome this issue using a multiscale approach.

The first part of the thesis establishes the close relation between computational grids in multiscale modeling and sampling strategies developed in information theory. The theory developed is based on the mathematical analysis

of multiscale functions of the type that are studied in averaging and homogenization theory and in multiscale modeling. Typical examples are two-scale functions $f(x, x/\epsilon)$, $(0 < \epsilon \ll 1)$ that are periodic in the second variable. We prove that under certain band limiting conditions these multiscale functions can be uniquely and stably recovered from nonuniform samples of optimal rate.

In the second part, we present a new multiscale approach for inverse homogenization problems. We prove that in certain cases where the specific form of the multiscale coefficients is known *a priori*, imposing an additional constraint of a microscale parametrization results in a well-posed inverse problem. The mathematical analysis is based on homogenization theory for partial differential equations and classical theory of inverse problems. The numerical analysis involves the design of multiscale methods, such as the heterogeneous multiscale method (HMM) [32]. The use of HMM solvers for the forward model has unveiled theoretical and numerical results for microscale parameter recovery, including applications to inverse problems arising in exploration seismology and medical imaging.

Table of Contents

List of Tables

List of Figures

Chapter 1

Introduction

This dissertation focuses on inverse problems for multiscale partial differential equations (PDEs) in which solution data is used to determine coefficients in the equation. PDE-constrained inverse problems involve many computational difficulties, in particular when the coefficients are of multiscale form. Two major challenges are addressed in this work by introducing theoretical and numerical strategies for multiscale inverse problems and then providing theoretical justification of the representation of multiscale functions using sampling theory corresponding to the numerical methods.

The scientific motivation for this work is the problem of obtaining high resolution images of a medium that has a microstructure. Examples that will be considered come from medical imaging of biological tissue, and reflection seismology, where the aim is to image the layered structure of the subsurface (see Figure 1.1). The goal is to use some knowledge of microstructure in the inversion process. To do so, we will consider model problems involving periodic microstructures that are designed to mimic target applications in medical imaging and reflection seismology. The periodicity assumption is made in order to use the mathematical tools available for the asymptotic analysis of periodic

structures.

Figure 1.1: **Microstructure imaging**. Left: Microscopy image of subcutaneous fat layer in mouse skin [43] (Image courtesy of Chris Freudiger, Wei Min, Brain Saar, Harvard University). Right: a 3D reflection profile of a polygonal faulted interval from seismic data [20] (Image courtesy of Joe Cartwright).

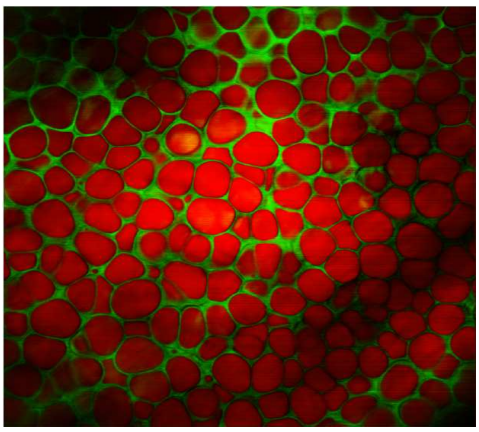

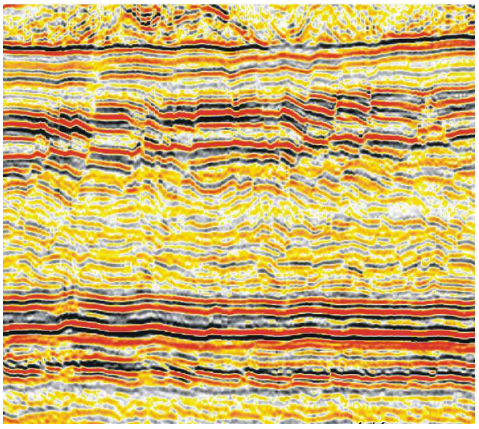

For an open, bounded domain, $\Omega \subset \mathbb{R}^d$, consider the model equation

$$-\nabla \cdot (a^\epsilon(x)\nabla u^\epsilon(x)) + b^\epsilon(x)u^\epsilon(x) = f(x) \text{ in } \Omega, \tag{1.0.1}$$

where the constant $\epsilon \ll 1$ represents the ratio of scales in the problem, and $a^\epsilon(x)$ and $b^\epsilon(x)$ posess variations on the ϵ—scale. When faced with balancing computational cost with accuracy, most approaches only deal with scientific models of large scale behavior and, for example, account for microscopic processes by using effective or homogenized equations to simplify computations.

Homogenization theory [15, 51] provides the form of the effective problem corresponding to (1.0.1); as $\epsilon \to 0$, $u^\epsilon \rightharpoonup U$ in $H^1(\Omega)$, where U solves

$$-\nabla \cdot (A(x)\nabla U(x)) + \overline{b}(x)U(x) = f(x) \text{ in } \Omega, \tag{1.0.2}$$

where the theory gives a constructive definition of A and $\overline{b}$.

The full inverse problem for (1.0.1) can be formulated as the minimization of the least-squares distance between predictions of the forward model and observed data. Direct inversion has a high computational cost and is typically ill-posed; a number of different sequences a^ϵ give the same limiting solution U, $\lim_{\epsilon\to 0} u^\epsilon = U$. In [70], the forward model in the full inverse problem is replaced by the homogenized equation corresponding to (1.0.1). This approach has a lower computational cost, however it does not guarantee recovery of the original multiscale coefficients.

Our approach is to include micro scales in the inversion by assuming that the unknown coefficient a^ϵ is completely determined by a function m through a bijective mapping $m \to a^\epsilon(m)$. The previous inverse problems can then be formulated in terms of microstructure, allowing for a constrained problem with fewer unknowns. Often, the explicit form of the homogenized coefficient corresponding to a^ϵ is not known, and therefore predictions of $A(m)$ cannot be computed. This issue is addressed numerically using the heterogeneous multiscale method, or HMM, introduced by E and Engquist [32]. HMM provides a framework for the design of methods that capture macroscale properties of a system using microscale information.

In this work a HMM forward solver is used to make effective predictions. Doing so increases the accuracy in the inversion process while benefiting from the low computational cost of a macroscale solver. In addition to numerical studies that illustrate the performance of these formulations, we will include

theoretical results that are motivated by inverse problems for (1.0.1) with $b^\epsilon = 0$ [3].

A major computational challenge is that in direct numerical simulation the smallest important scales must be resolved over the length of the largest scales in each dimension. Even the basic cost of direct numerical simulation can be understood from the viewpoint of information theory. The classical Shannon sampling theorem states that in order to represent the solution, at least two unknowns per wavelength is required [76]. If the size of the computational domain is 1 and $\epsilon \ll 1$ is the smallest important wave length, then at least $2\epsilon^{-1}$ unknowns are required in each dimension. The computational complexity in d dimensions must then be at least $O(\epsilon^{-d})$.

If this is too much for the available computational resources, then some special features of the original problem must be exploited. Scale separation is assumed in homogenization theory [15] and in convergence analysis of HMM [63]. The functions involved are typically of the form

$$f^\epsilon(x) = f(x, x/\epsilon) \qquad \text{where } f(x,y) \text{ is periodic in } y, \quad 0 < \epsilon \ll 1.$$

With equidistant sampling points the rate must still be the same as above, $O(\epsilon^{-d})$, in order to recover the function. Different sampling strategies are required to exploit the special structure of the functions. This corresponds to strategies for numerical computational grids in multiscale simulations.

Chapter 2 describes the homogenization theory used to develop effective models for multiscale systems. In Chapter 3 the abstract HMM framework is

described as well as an outline of a typical HMM scheme for elliptic partial differential equations. In Chapter 4 we prove that some techniques of multiscale computations actually are optimal if seen via information theory and sampling theory. In Chapter 5, we apply homogenization theory and multiscale numerical methods to inverse problems for PDEs with oscillatory coefficients. Chapters 4 and 5 are parts of submitted manuscripts. We conclude and describe future directions in Chapter 6.

Chapter 2

Homogenization

Multiscale problems arising in science and engineering can involve complex relationships between processes occurring on different spatial and temporal scales. An example is the solution of boundary value problems in periodic heterogeneous media, where the size of the heterogeneities, denoted ϵ, may be much smaller than the size of the domain. Often, we desire a global view of the behavior of the solution in a homogeneous domain.

The mathematical framework developed for these problems is called *averaging* or *homogenization*. Homogenization theory provides a way to extract effective properties of the microscopic solution of the unit cell (micro) problem and translate these properties into parameters for the global (macro) problem. This is done using an asymptotic analysis of the microscopic model. The effective model then describes solutions to the boundary value problem as $\epsilon \to 0$.

It should be noted that homogenization theory extends to more general classes of problems. The most general theory in homogenization was first introduced as $G-$ convergence by Spagnolo [79, 80], and later generalized by Tartar [83] and Murat and Tartar [65] as $H-$convergence. Homogenization theory is also developed in the variational setting of $\Gamma-$convergence [27, 26, 18] and in

terms of 2—scale convergence in [4]. See [4, 23, 25, 37, 51, 65, 69] for further details about these techniques.

We focus here on *periodic homogenization* for partial differential equations in order to relate the mathematical theory to physical applications involving media with periodic or locally periodic microstructures. The study of periodic structures using asymptotic analysis can be found in the works of Babuska [5, 6, 7, 8] and Bensoussan, Lions, and Papanicolau [15]. Periodic homogenization is rigorously justified through H—convergence.

2.1 Homogenization of elliptic equations

We start with some basic definitions and notation to describe Sobolev spaces of periodic functions.

Definition 2.1.1. Let X be a Banach space with norm $\|\cdot\|_X$ and let Ω denote an open subset of $\mathbb{R}^d$. The space $Y := L^2(\Omega;X)$ consists of all measurable functions $u : x \in \Omega \to u(x) \in X$ such that $\|u(x)\|_X \in L^2(\Omega)$.

The space $Y = L^2(\Omega;X)$ is equipped with the norm

$$\|u\|_Y = \left(\int_\Omega (\|u(x)\|_X)^2 \, dx \right)^{1/2}.$$

These ideas can be generalized to $H^1(\Omega;X)$. See [69] for more details. We will denote the d—dimensional unit torus, or the *unit cell* by $\mathbb{T}^d$.

Definition 2.1.2. Functions $f : \mathbb{R}^d \to \mathbb{R}$ that satisfy

$$f(y + e_i) = f(y) \quad \forall y \in \mathbb{R}^d, i \in \{1, \ldots, d\},$$

where $\{e_i\}$ is the standard basis for $\mathbb{R}^d$, are called 1—*periodic functions*.

Then $C^\infty_{per}(\mathbb{T}^d)$ is the restriction to $\mathbb{T}^d$ of smooth functions in $C^\infty(\mathbb{R}^d)$ that are 1—periodic. The spaces $L^p_{per}(\mathbb{T}^d)$ are defined to be the completion of $C^\infty_{per}(\mathbb{T}^d)$ with respect to the L^p—norm. The same holds for $H^1_{per}(\mathbb{T}^d)$.

In periodic homogenization of functions of two scales, it is common for multiscale functions to be constructed from functions $u(x, y)$ that are periodic in the second variable. Then, setting $u^\epsilon(x) = u(x, x/\epsilon)$ produces a function that has a highly oscillatory component on the ϵ—scale.

Definition 2.1.3. *Locally periodic* functions are functions that belong to the space $L^2(\Omega; C^\infty_{per}(\mathbb{T}^d))$ equipped with the norm

$$\|u\|_{L^2(\Omega; C^\infty_{per}(\mathbb{T}^d))} = \left(\int_\Omega \left(\sup_{y \in \mathbb{T}^d} |u(x, y)| \right)^2 dx \right)^{1/2}.$$

The following theorem (see [69]) is used to relate the convergence properties of u^ϵ in the space $L^2(\Omega)$ to the convergence of locally periodic functions $u(x, y)$.

Theorem 2.1.1. *Let $u \in L^2(\Omega; C_{per}(\mathbb{T}^d))$, $\epsilon > 0$, and $u^\epsilon(x) = u(x, x/\epsilon)$. Then*

(i) $u^\epsilon \in L^2(\Omega)$ and $\|u^\epsilon\|_{L^2(\Omega)} \leq \|u\|_{L^2(\Omega, C_{per}(\mathbb{T}^d))}$,

(ii) u^ϵ converges to $\int_{\mathbb{T}^d} u(x, y) dy$ weakly in $L^2(\Omega)$ as $\epsilon \to 0$,

(iii) As $\epsilon \to 0$, $\|u^\epsilon\|_{L^2(\Omega)} \to \|u\|_{L^2(\Omega\times\mathbb{T}^d)}$.

We remark that the homogenization theory presented next can be extended to functions with lower regularity and refer to the references [51, 69] for further reading.

Elliptic differential operators in divergence form

We let $\Omega \subset \mathbb{R}^d$ be an open, bounded domain with smooth boundary $\partial\Omega$. We will consider solutions $u^\epsilon \in H^1(\Omega)$ to the Dirichlet problem

$$\begin{cases} -\nabla\cdot(a^\epsilon \nabla u^\epsilon) + b^\epsilon u^\epsilon = f, & \text{in } \Omega, \\ u^\epsilon = 0, & \text{in } \partial\Omega, \end{cases} \tag{2.1.1}$$

for a source term $f \in L^2(\Omega)$ and $a^\epsilon(x) = \{a_{ij}(x, x/\epsilon)\}$ and $b^\epsilon(x) = b(x, x/\epsilon)$ for locally periodic functions $a_{ij}(x,y)$ and $b(x,y)$. Furthermore, we assume that $a(x,y) = \{a_{ij}(x,y)\}$ is a uniformly positive definite, symmetric matrix function with bounded elements.

The goal of homogenization is to describe the limiting behavior of solutions to the family of problems (2.1.1). Classical results [51, 69] state that as $\epsilon \to 0$, $u^\epsilon \to U$, where $U \in H^1(\Omega)$ is a solution to the *effective* or *homogenized* equation of the form

$$\begin{cases} -\nabla\cdot(A\nabla U) + \overline{b}U = f, & \text{in } \Omega, \\ U = 0, & \text{in } \partial\Omega. \end{cases} \tag{2.1.2}$$

The source term f is assumed to be a function that contains variations on the slow scale, and the homogenized coefficients A and $\overline{b}$ are independent of ϵ. Also, A is a symmetric, uniformly positive definite matrix function.

Theorem 2.1.2 (Classical homogenization of elliptic equations). *Let u^ϵ be the weak solution of the multiscale problem (2.1.1) and let U be the weak solution to the homogenized problem (2.1.2) with coefficients $A(x)$ and $\overline{b}(x)$ defined for each x in Ω by the formulas*

$$A(x) = \int_{\mathbb{T}^d} \left(a(x,y) + a(x,y)\nabla\chi(x,y)^T\right) dy, \tag{2.1.3}$$

$$\overline{b}(x) = \int_{\mathbb{T}^d} b(x,y)dy, \tag{2.1.4}$$

where the vector field $\chi : \Omega \times \mathbb{T}^d \to \mathbb{R}^d$ is a weak solution to the following cell problem *for each $x \in \Omega$*

$$\begin{cases} -\nabla_y \cdot \left(\nabla_y \chi(x,y) a(x,y)^T\right) = \nabla_y \cdot a(x,y)^T, \\ y \to \chi(x,y) \text{ is } 1-\text{periodic}. \end{cases} \tag{2.1.5}$$

Then, the following convergence holds:

1. *$u^\epsilon \rightharpoonup U$ weakly in $H_0^1(\Omega)$;*
2. *$u^\epsilon \to U$ strongly in $L^2(\Omega)$;*
3. *$a^\epsilon \nabla u^\epsilon + b^\epsilon u^\epsilon \to A\nabla U + \overline{b}U$ weakly in $L^2(\Omega)$.*

Remark 2.1.1. In one dimension the coefficients can be explicitly computed using the formulas

$$A(x) = \left(\int_0^1 a(x,y)^{-1} dy\right)^{-1}, \qquad \overline{b}(x) = \int_0^1 b(x,y)dy. \tag{2.1.6}$$

Note that this expression requires the evaluation of the integrals in (2.1.6) for each $x \in \Omega$. If we restrict ourselves to functions $a^\epsilon(x) = a(x/\epsilon)$ and $b^\epsilon(x) =$

$b(x/\epsilon)$ for functions a and b that are both 1—periodic, the formulas are simplified. In this case A is a constant function equal to the harmonic mean of a and $\overline{b}$ is a constant function equal to the arithmetic mean of b.

The homogenized equation in higher dimensions can be formally derived using the method of matched asymptotics, where it is assumed *a priori* that solutions of the Dirichlet problem (2.1.1) have a decomposition of the form

$$u^\epsilon(x) = u_0(x,y) + \epsilon u_1(x,y) + \epsilon^2 u_2(x,y) + \dots \text{ where } y = \epsilon^{-1}x. \qquad (2.1.7)$$

The functions $u_0, u_1, u_2, \dots$ are assumed to be locally periodic. Since differentiation of the right hand side of (2.1.7) can be expressed as

$$\nabla = \nabla_x + \epsilon^{-1}\nabla_y,$$

it follows that the differential operator L^ϵ corresponding to (2.1.1) applied to functions with representation (2.1.7) can be written as

$$\begin{aligned} L^\epsilon u^\epsilon - f =& \epsilon^{-2} L_1 u_0 + \epsilon^{-1}(L_1 u_1 + L_2 u_0) \\ &+ \epsilon^0 (L_1 u_2 + L_2 u_1 + L_3 u_0 - f) \\ &+ \epsilon (L_1 u_2 + L_2 u_2 + L_3 u_1) + O(\epsilon^2), \end{aligned}$$

where the operators L_1, L_2, and L_3 are defined by

$$\begin{aligned} L_1 &= -\nabla_y \cdot \big(a(x,y)\nabla_y\big), \\ L_2 &= -\nabla_y \cdot (a(x,y)\nabla_x) - \nabla_x \cdot \big(a(x,y)\nabla_y\big), \\ L_3 &= -\nabla_x \cdot (a(x,y)\nabla_x) + b(x,y). \end{aligned}$$

Collecting $O(\epsilon^{-2})$, $O(\epsilon^{-1})$, and $O(1)$ terms in the expression for L^ϵ produces a system of equations with the unknowns u_0, u_1, and u_2. Enforcing that the compatibility conditions of the Fredholm alternative are satisfied leads to the condition $u_0 = U$ and A, $\overline{b}$ as in Theorem 2.1.2.

The method of matched asymptotics does not provide a rigorous homogenization result, rather a guide to deriving the homogenized equation. In general, there is no way of ensuring that u^ϵ has the multiscale decomposition (2.1.7). Techniques for proving 2.1.2, include two-scale convergence, Γ—convergence, and G—convergence. A review of the general theory can be found in the homogenization literature [4, 23, 37, 51, 69].

2.2 Discussion, related issues

The given expression for A is implicit and determined by solutions to the cell problems. There are special cases where the explicit form of A is known, including the one-dimensional case and homogenized equations for layered materials in higher dimensions. In d dimensions, layered materials are modeled using a coefficient of the form $a^\epsilon(x) = a(y/\epsilon)$, where the matrix a is a function of y_1 only, that is, $a_{ij}(y) = a_{ij}(y_1), \quad i, j = 1, 2, \ldots, d$. For more general problems, the homogenized coefficients cannot be explicitly computed; however, theoretical bounds on the coefficients can be obtained. Homogenization for locally periodic structures is developed in [75].

In practice, numerical homogenization techniques such as upscaling are

Figure 2.1: **Periodic homogenization.** Plots of the full solution (left) and homogenized solution (right) of the multiscale elliptic equation (2.1.1).

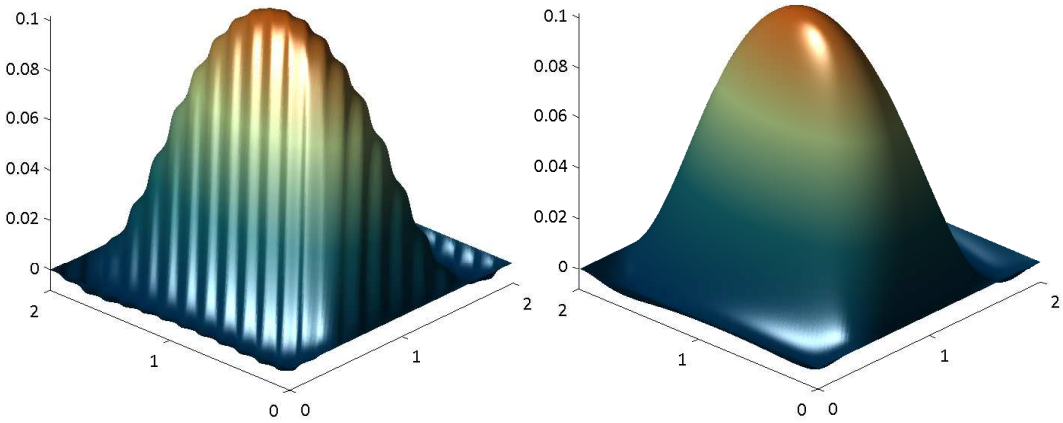

used to determine effective solutions. Figure 2.1 contains a plot of the multiscale solution to (2.1.1) and the homogenized solution using the finite element method with piecewise linear basis functions. In order to resolve the full solution, a triangulation must contain elements of size $h < \epsilon$. The homogenized solution, independent of epsilon, is resolved on a triangulation with elements of size $H > \epsilon$.

Chapter 3

Heterogeneous Multiscale Methods (HMM)

A main challenge in multiscale modeling is in overcoming the high computational cost of direct simulation. One way around this is to use an effective equation to describe the system that is derived from averaging or homogenization techniques.The heterogeneous multiscale method (HMM) was introduced in [32] to provide a framework for modifying existing methods in order to efficiently handle multiscale problems. The HMM philosophy is to approximate the solution to a macroscale model by judiciously extracting needed information from the microscale model, allowing for an exchange of information between the solvers as needed. HMM has been applied to multiscale partial differential equations, including elliptic problems, parabolic problems, wave equations, ordinary differential equations, and stochastic problems [1, 35, 31].

3.1 Abstract framework

The main goal of HMM is to design methods that capture the effective properties of a multiscale system without full knowledge of the effective model. We think of $\{U\}$ as the set of *macroscopic* state variables of interest, defined on a macroscopic computational domain Ω_H with step size H. At our disposal is a

fine-scale model that describes the set of *microscopic* state variables $\{u\}$ that are defined on a microscopic domain Ω_h with step size h.

The relationship between the macroscale solution U and the microscale solution u can be described using operators for compression and reconstruction, denoted, Q and R respectively, that satisfy

$$Qu = U, \quad RU = u.$$

In order for consistency, Q and R must satisfy $QRU = U$ for all macroscopic solutions U. Examples of Q include projection and coarse-graining, and we usually think of Q as a linear operator, though this is not always the case. There is no unique way to define the reconstruction operator R. Examples of compression and reconstruction operators are given in [32].

HMM is used for a class of multiscale problems where it is assumed that a macroscale model C describes the macroscopic state variable U through the state equation

$$C(U, D) = 0. \tag{3.1.1}$$

Here, D denotes the data needed for the macroscale model to be complete. This data is dependent on the microscale variable, in other words $D = D(u)$, where u solves the microscopic state equation

$$c(u, d) = 0, \tag{3.1.2}$$

where the relationship $d = d(U)$ represents the data needed from the macroscale model in order to compute microscale simulations.

HMM is designed for problems where the goal is to determine the macroscopic solution U when C is known except for the missing parameter D, which is estimated using a known microscale model c, and the constitutive relationship between the models. The main components of HMM follow.

1. *A macroscopic solver*. The macroscale model (3.1.1) is assumed to be known except for the missing parameter D. The knowledge of the form of C allows for us to select an appropriate solver for the macroscale model.

2. *A way to estimate missing parameters in the macroscale model*. The assumptions of scale separation allow us to use microscale simulations in order to estimate D. This can be done "on the fly" or as a pre-processing step. There are two steps.

   (a) *Constrained microscale simulation*. Here the microscopic model given in (3.1.2) is solved by enforcing compatibility conditions with the macroscopic solution through the constraint $d = d(U)$. Examples of these compatibility conditions are initial data or boundary conditions, and in practice this is where most of the technical difficulties lie.

   (b) *Data processing*. Once the microscale solution to (3.1.2) is known, the macroscale parameter $D = D(u)$ can be estimated and then substituted into the effective model (3.1.1).

The main difficulty of HMM is the notion of a preconceived macroscale model. In our setting of elliptic partial differential equations, homogenization

theory is used to derive the effective equation, however it should be noted that HMM is a framework for the design of multiscale methods, and the effective equation can be obtained through other means.

3.2 HMM for second order elliptic equations

Here we will consider the classical elliptic equation for a domain $\Omega \subset \mathbb{R}^d$

$$\begin{cases} -\nabla \cdot (a^\epsilon(x)\nabla u^\epsilon(x)) = 0, & \text{in } \Omega \\ u^\epsilon(x) = 0, & \text{in } \partial\Omega. \end{cases} \tag{3.2.1}$$

One class of methods developed for these problems is the multiscale finite element method (MsFEM) [33, 48]. MsFEM involves a discretization of the full problem (3.2.1) and the use of multiscale basis functions that resolve details of the solution at all scales. Therefore, the computational complexity is proportional to the number of unknowns in the fine scale problem. If the chief concern is the resolution of the effective properties of the solution, a reduced model can be used to simplify computations.

The multiscale problem (3.2.1) is well studied in homogenization theory [15, 51] and is commonly used to demonstrate techniques in multiscale computation. The homogenized equation corresponding to (3.2.1) is of the form

$$\begin{cases} -\nabla \cdot (A(x)\nabla U(x)) = 0, & \text{in } \Omega \\ U(x) = 0, & \text{in } \partial\Omega. \end{cases} \tag{3.2.2}$$

Numerical methods such as the finite element heterogeneous multiscale method (FE-HMM) [1, 32] approximate the solution to an effective problem (3.2.2) using grids with typical macroscale spacing $H > \epsilon$. A main advantage

of FE-HMM is that only partial knowledge of the homogenized coefficient is needed.

In the basic setting for FE-HMM, the macroscale model is $F = F(U,A)$, and the missing data is A, the effective coefficient. Figure 3.1 contains a diagram of the coupled macro-micro grids used in a typical FE-HMM scheme.

1. **Macro model discretization**. First, the effective model (3.2.2) is discretized using a finite element space X_H corresponding to the triangulation $\mathcal{T}_H$ of the domain Ω containing of element size H. The resulting macroscale bilinear form is defined for functions V and W lying in the finite element space X_H, and it is

$$\mathcal{B}(V,W) := \int_\Omega \nabla V(x) \cdot A_{HMM}(x) \nabla W(x) dx,$$

where A_{HMM} is not known explicitly. This term is approximated using numerical quadrature for a set of quadrature points, $\{x_l\}$, and weights, $\{\omega_l\}$,

$$\mathcal{B}(V,W) \simeq \sum_{K \in \mathcal{T}_H} |K| \sum_{x_l \in K} \omega_l \left(\nabla V \cdot A_{HMM} \nabla W\right)(x_l), \tag{3.2.3}$$

where $|K|$ is the measure of K.

2. **The micro solver**. For $V \in X_H$, the stiffness matrix entries $\mathcal{B}(V,V)$ are computed using a microscale solver when the effective coefficient A_{HMM} is not known. The effective behavior of a^ϵ is captured locally by solving cell problems. The microscopic model is $f(v_l^\epsilon, v_l^\epsilon|_{\partial I_\delta(x_l)}) = 0$, where v_l^ϵ is the solution to

$$-\nabla \cdot (a^\epsilon \nabla v_l^\epsilon) = 0 \text{ in } I_\delta(x_l) := x_l \pm \tfrac{\delta}{2} I, \tag{3.2.4}$$

with the boundary conditions dependent on V. There are three formulations of the local microscale problem.

i. The Dirichlet formulation for the local microscale problem (3.2.4) imposes the boundary conditions

$$v_l^\epsilon(x) = V(x) \text{ on } \partial I_\delta(x_l).$$

ii. The Neumann formulation for the local microscale problem (3.2.4) imposes the boundary conditions

$$a^\epsilon \nabla v_l^\epsilon \cdot n = \lambda \cdot n \text{ on } \partial I_\delta(x_l)$$

where λ is the constant Lagrange multiplier for the constraint

$$\langle \nabla v_l^\epsilon \rangle_{I_\delta(x_l)} = \langle \nabla V \rangle_{I_\delta(x_l)}.$$

iii. The periodic formulation for the local microscale problem (3.2.4) imposes the boundary conditions

$$v_l^\epsilon - V \text{ is } I_\delta(x_l) - \text{ periodic.}$$

In this work, a $\mathcal{P}_1$ finite element method is chosen with triangulations $\mathcal{T}_h^l$ of the subdomains $I_\delta(x_l)$. The spacing $h < \epsilon$ is chosen sufficiently small in order to resolve the microscale.

3. **Reconstruction step**. Then, the term $(\nabla V \cdot A_{HMM} \nabla W)(x_l)$ in (3.2.3) can be estimated by

$$(\nabla V \cdot A_{HMM} \nabla W)(x_l) \simeq \frac{1}{\delta^n} \int_{I_\delta(x_l)} \nabla v_l^\epsilon \cdot (a^\epsilon \nabla w_l^\epsilon) dx.$$

The HMM bilinear form is then defined by

$$\mathcal{B}_{HMM}(V,W) := \sum_{K\in\mathcal{T}_H} \frac{|K|}{\delta^n} \sum_{x_l\in K} \omega_l \int_{I_\delta(x_l)} \nabla v_l^\epsilon \cdot (a^\epsilon \nabla w_l^\epsilon) dx. \tag{3.2.5}$$

Finally, the HMM solution, U_{HMM}, solves the problem

$$\min_{V\in X_H} \frac{1}{2}\mathcal{B}_{HMM}(V,V) - (f,V).$$

Figure 3.1: **FEM-HMM Discretization.** An illustration of HMM for divergence form PDEs. The orange dotted lines represent the macroscopic computational domain $\mathcal{T}_H$. The collection of light blue boxes represent the microscopic computational domains $\mathcal{T}_h^l$ centered at the points x_l.

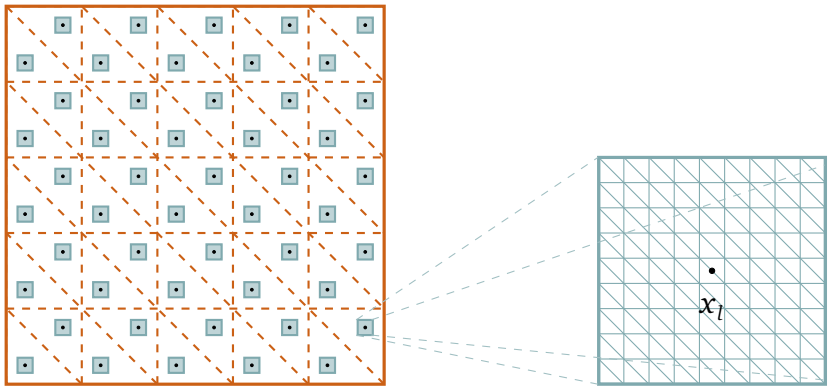

The cell size δ and the boundary conditions in (3.2.4) can vary. See [96] for results on the effects of the different boundary conditions and cell size on the estimate of the effective coefficients. Periodic conditions were found to give the best performance; in general, Neumann boundary conditions result in an underestimation of the effective coefficient and Dirichlet conditions result in and overestimation. The effects of cell size and boundary conditions on the error associated with HMM are plotted in Figures 3.2 and 3.3.

Implementation

An implementation of HMM for the problem (3.2.1) is given by Algorithm 1 and Algorithm 2. Here, the macroscale model and microscale model are both discretized using the finite element method. The macroscale triangulation $\mathcal{T}_H$ contains elements of size H, and the microscale triangulation $\mathcal{T}_h$ contains elements of size h, with $H > \epsilon$ and h chosen small enough that it resolves the $\epsilon-$scale.

Macro solver. Algorithm 1 contains a solver for the equation $C(U^{HMM}, D) = 0$ given by (3.1.1). This algorithm requires inputs of the coefficient a^ϵ in the microscale equation (3.1.2) and H and h, the resolution of the coarse and fine meshes.

- On **line 2**, the variables initialized are the macroscale triangulation $\mathcal{T}_H$ of the domain Ω and the set of finite element basis functions X_H. In our numerical simulations, piecewise-linear basis functions are used.

- At this point, a basic finite element formulation can be used to solve the homogenized problem (3.1.1) if there is knowledge of A. Since a^ϵ is not assumed to be periodic, there may be no way to determine A directly from A, so constrained microscale simulation must be used to estimate A. In order to reduce computational cost, the stiffness matrix contribution of A will be estimated for certain values in the domain. On **line 3** the values

for the nodes and weights corresponding to the quadrature formula (3.2.3) are stored.

- Then, on **lines 4 − 6** a microscale solver is used to estimate D, the entries of the macroscale stiffness matrix.

- Once the missing information D is estimated, the model $C(U^{HMM}, D) = 0$ is solved on **lines 7 − 8**.

Microscale solver. A finite element formulation is chosen to solve the microscale cell problems (3.2.4) with constraints given by the macroscale basis functions V and W in X_H. The pseudo code is given in Algorithm 2.

- The for loop in **lines 2 − 9** is used to store each approximation of the quantity $(\nabla W \cdot A_{HMM} \nabla V)(x)$ at each quadrature node in the set $\{x_l\}$.

- The local subdomains $I_\delta(x_l)$ are initialized on **line 3**.

- Then, on **lines 4 − 5** the functions V and W are used to create constraints for the microscale simulations of the form $d = d(V)$ and $d = d(W)$. Here, the constraints are in the form of boundary conditions.

- The cell problems are solved on **lines 6 − 7** using an $O(h)$ triangulation of the subdomain $I_\delta(x_l)$.

- On **line 10**, the quadrature formula is applied using the given weights and nodes. This is the data processing step, $D = D(u)$.

Algorithm 1 FE-HMM scheme

function HMMSOLN(a^ϵ, H, h)
  $(X_H, \mathcal{T}_H) =$ ELEMENTBASIS(H)
  $\{(x_l, \omega_l)\} =$ QUADFORMULA($\mathcal{T}_H$)
  for all V_j, V_k in X_H **do**
    $D_{jk} \leftarrow$ MICROSOLVER(a^ϵ, h, (V_j, V_k), $\{(x_l, \omega_l)\}$)
  end for
  $U^{\text{HMM}} \leftarrow$ MACROSOLVER(D, $\mathcal{T}_H$)
  return U^{HMM}
end function

Algorithm 2 Constrained microscale simulation and data processing

function MICROSOLVER(a^ϵ, h, (V, W), $\{(x_l, \omega_l)\}$)
  for all x_l **do**
    $I_\delta = x_l \pm \frac{\delta}{2} I$
    $g_v = \text{BC}(V, I_\delta)$
    $g_w = \text{BC}(W, I_\delta)$
    $v^\epsilon =$ CELLSOLN(a^ϵ, g_v, h)
    $w^\epsilon =$ CELLSOLN(a^ϵ, g_w, h)
    $Q_l \leftarrow \frac{1}{\delta^d} \int_{I_\delta} \nabla w^\epsilon \cdot a^\epsilon \nabla v^\epsilon dx$
  end for
  $D \leftarrow$ QUAD($\{Q_l\}$, $\{(x_l, \omega_l)\}$)
  return D
end function

3.3 Computational complexity and error estimates

Because HMM involves different models for the macroscale state and the microscale state, the numerical analysis of HMM depends on the choice of solvers. Instead, a general result for error estimates resulting from HMM discretizations has been developed in [32] for so-called "Type B" problems, where it is assumed that a microscale model exists but is either partially known or

computationally expensive to directly compute.

This research primarly involves the application of HMM to elliptic PDEs, so we will present relevant numerical analysis for elliptic homogenization problems in Ming and Zhang [63]. Here it is assumed that the HMM macroscale model is solved with an order k scheme on a computational domain with resolution H.

Theorem 3.3.1 (Ming, Zhang 2005). *Denote by U, U_{HMM} the solutions to (3.2.2) and the HMM solution, respectively. Let*

$$e(HMM) = \max_{x_l \in K, K \in \mathcal{T}_H} \|A(x_l) - A_{HMM}(x_l)\|,$$

where $\|\cdot\|$ is the Euclidean norm. If U is sufficiently smooth, and $\lambda I \leq a^\epsilon \leq \Lambda I$ for $\lambda, \Lambda > 0$, then there exists a constant C independent of ϵ, δ and H such that

$$\|U - U_{HMM}\|_1 \leq C\left(H^k + e(HMM)\right),$$
$$\|U - U_{HMM}\|_0 \leq C\left(H^{k+1} + e(HMM)\right).$$

It should be noted that there is no assumption of periodicity of a^ϵ in Theorem 3.3.1, and U could refer to a solution to an arbitrary partial differential equation of the form (3.2.2). However, in order to enforce $U_{HMM} \to U$ as $e(HMM) \to 0$, the function U is chosen to be the unique solution to the homogenized equation.

For periodic homogenization problems, as described in the previous chap-

ter, the error introduced by an HMM discretization can be quantified by

$$e(HMM) \leq \begin{cases} C\epsilon & I_\delta(x_l) = x_l + \epsilon I \\ C(\frac{\epsilon}{\delta} + \delta) & \text{otherwise.} \end{cases}$$

Example 1. Here the FEM-HMM solution is computed using a macroscopic triangulation $\mathcal{T}_H$. The local cell problem with Dirichlet boundary conditions is solved on subdomains using an $O(h)$ microscopic computational domain $\mathcal{T}_h$. The model problem is (3.2.1) with a^ϵ defined by

$$a^\epsilon(x) = 1 + .5\sin(2\pi x_2/\epsilon).$$

The explicit form of the homogenized coefficient is known as

$$A = \begin{pmatrix} \langle a^\epsilon \rangle_{\mathbb{T}^2} & 0 \\ 0 & \langle (a^\epsilon)^{-1} \rangle_{\mathbb{T}^2}^{-1} \end{pmatrix},$$

where the averaging operator is denoted $\langle \cdot \rangle_Y$, $\langle g \rangle_Y = \frac{1}{|Y|} \int_Y g(y) dy$. Direct computation of U, the solution to the homogenized equation (3.2.2), is done using the finite element method on Ω_H. Then, the HMM solution U_{HMM} and the true homogenized solution U can be compared. In Figures 3.2 and 3.3 the quantity $\|U_{HMM} - U\|$ is plotted as the cell size and macroscopic mesh size are varied.

Figure 3.2: **Error from varying cell size.** The HMM error is computed for varying microscopic cell sizes δ. The plot describes the error for each cell size ratio δ/ϵ using both the Dirichlet and Neumann formulations of the cell problem (3.2.4).

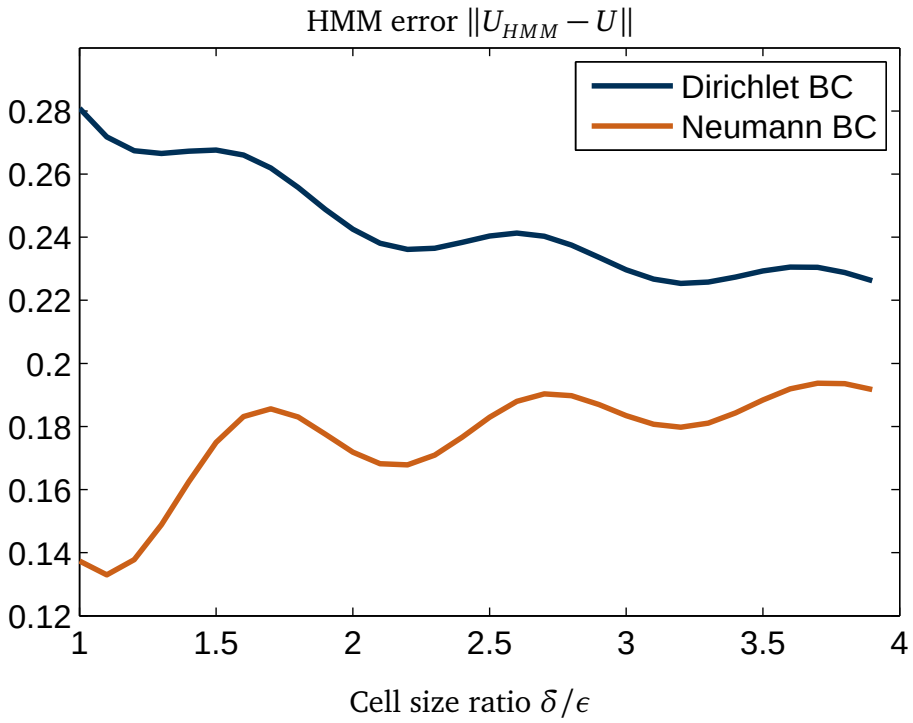

Figure 3.3: **Error from varying** H. The error in the HMM solution U_{HMM} for the effective solution of the multiscale problem (3.2.1) is plotted against the macroscopic mesh size $H > \epsilon$. The HMM solution is compared with U, the solution to the homogenized problem (3.2.2).

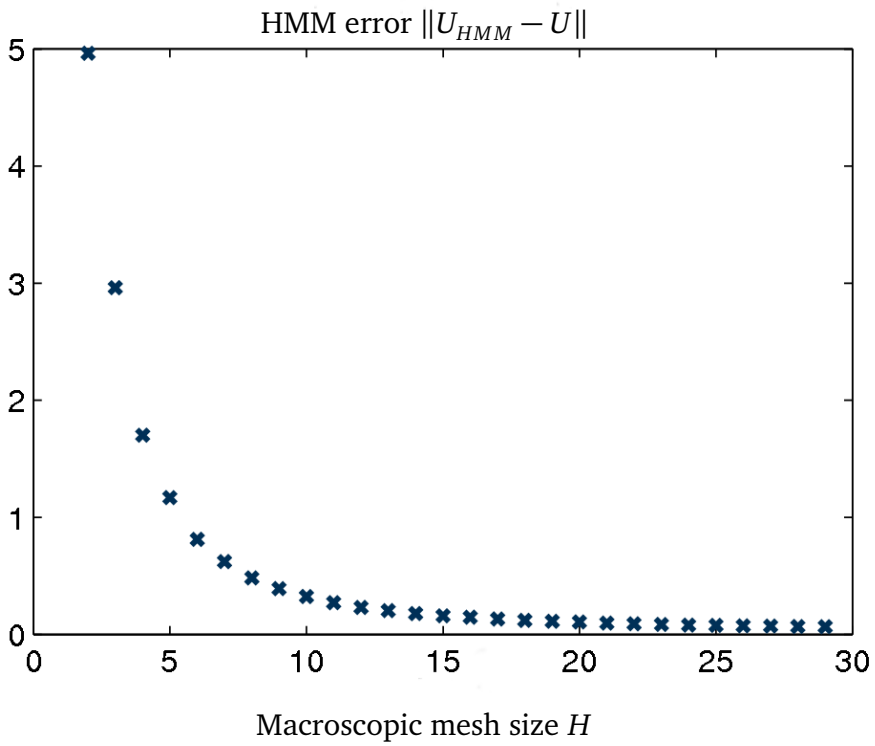

Chapter 4

Nonuniform sampling and multiscale computation

Multiscale modeling and computation has recently been a very active research field. A major computational challenge is that in direct numerical simulation the smallest important scales must be resolved over the length of the largest scales in each dimension. This can lead to a prohibitively high computational cost. A number of different numerical frameworks have been proposed to handle this problem and we will here focus on the heterogeneous multiscale method (HMM) [1, 32]. The purpose of this work is to study multiscale modeling from the point of view of information theory.

Even the basic cost of direct numerical simulation can be understood from information theory. The classical Shannon sampling theorem states that in order to represent the solution, at least two unknowns per wavelength is required [76]. If the size of the computational domain is 1 and $0 < \epsilon \ll 1$ is the smallest important wave length, then at least $2\epsilon^{-1}$ unknowns are required in each dimension. The computational complexity in d dimensions must then be at least $O(\epsilon^{-d})$.

If this is too much for the available computational resources then some special features of the original problem must be exploited. Scale separation is

assumed in homogenization theory, [4, 15, 51, 69], and in convergence analysis of HMM. The functions involved are typically of the form,

$$f^\epsilon(x) = f(x, x/\epsilon), \qquad f(x,y) \text{ is 1-periodic in } y, \quad 0 < \epsilon \ll 1. \tag{4.0.1}$$

With equidistant sampling points the rate must still be the same as above $O(\epsilon^{-d})$ in order to recover the function. Different sampling strategies are required to exploit the special structure of the functions. This corresponds to strategies for numerical computational grids in multiscale simulations. It will be seen that some techniques of multiscale computations actually are optimal if seen via information theory.

For $g \in L^2(\mathbb{R}^d)$ the Fourier transform, denoted $\hat{g} \in L^2(\mathbb{R}^d)$, is defined by

$$\hat{g}(\xi) = \int_{\mathbb{R}^d} g(x) e^{2\pi i x\cdot\xi} dx.$$

Here we will let x, y be points in $\mathbb{R}^d$, $x = (x_1, \ldots, x_d)$, $y = (y_1, \ldots, y_d)$. We will think of x, y as spatial variables, and think of $\xi = (\xi_1, \ldots, \xi_d)$ as a frequency variable. The dot product is defined as

$$\langle \xi, x \rangle = x_1\xi_1 \ldots x_d\xi_d.$$

Functions whose Fourier transforms have bounded support are called *bandlimited functions*.

The class of multiscale functions $f^\epsilon(x)$ defined by (4.0.1) possess scale separation between the $O(1)$ "slow" oscillations and $O(\epsilon^{-1})$ "fast" oscillations

when $f(x, y)$ is a bandlimited function in both variables. In the following, we make the assumption

$$f(x, y) \text{ is } \Omega \times \mathcal{M} - \text{bandlimited}, \tag{4.0.2}$$

where $\Omega \subset \mathbb{R}^d$ and $\mathcal{M} \subset \mathbb{Z}^d$ are bounded, measurable sets. We will see later that these conditions follow naturally from the periodicity assumption.

The spectrum of the function $f^\epsilon \in L^2(\mathbb{R})$ defined by (4.0.1) is supported on a finite union of intervals

$$\hat{f^\epsilon}(\xi) = 0 \text{ for all } \xi \notin \bigcup_{m \in \mathcal{M}} \left(\Omega + \frac{m}{\epsilon} \right). \tag{4.0.3}$$

This representation combines the two notions of "scale" used in information theory and in multiscale computation. The gaps between the spectral bands are a result of the scale separation assumptions on f^ϵ and f.

The spectral support of a one-dimensional signal that satisfies the above properties is illustrated in Figure 4.1. These functions are of much interest to the multiscale modeling community. A useful characteristic of these functions, that will be shown in the sequel, is that explicit knowledge of the locations of the frequency bands allows for the design of a sampling strategy to reconstruct f^ϵ using an optimal sampling rate. Specifically, for each fixed k in the bounded set $\mathcal{K} = \{k_1, k_2, \ldots, k_P\} \subset \mathbb{Z}^d$, the sampling sets X_k are given by

$$X_k = \{j\Delta x + k\delta x \mid j \in \mathbb{Z}^d\}, \qquad k \in \mathcal{K}, \tag{4.0.4}$$

where $\Delta x > \epsilon$ is the uniform gap between samples in the set X_k and $\delta x < \epsilon$ is a small perturbation.

Figure 4.1: **Multiband spectrum and nonuniform sampling set ($d = 1$).** The diagram below represents the spectral support of a one-dimensional function satisfying (4.0.3) (top) and nonuniform sampling points in the set $\mathcal{M} = \{0, \pm 1, , \ldots, \pm M\}$ (bottom).

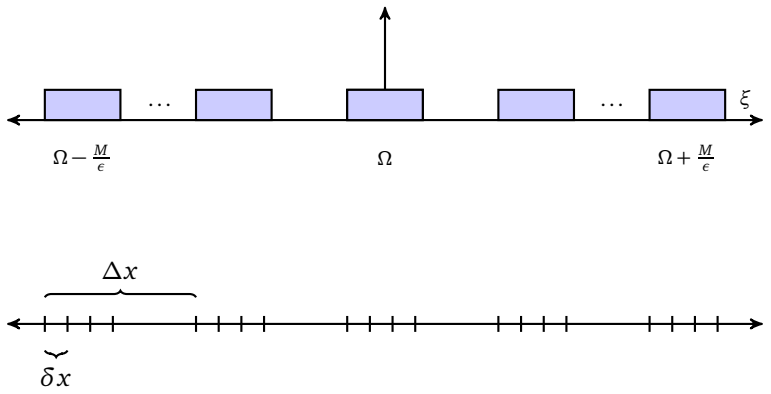

We will now state the main nonuniform sampling theorem for multiscale functions. The proof will be given in later sections.

Theorem 4.0.1. *For $d = 1$ let $\Omega \subset \mathbb{R}$ be a bounded interval and let $\mathcal{M} \subset \mathbb{Z}$ be bounded set of frequencies. Suppose that f^ϵ is a function of the form (4.0.1), for a function f satisfying (4.0.2). Let Δx satisfy $0 < \Delta x < \frac{1}{|\Omega|}$ and let δx satisfy $0 < \delta x < \epsilon/M$, where $M \geq \sup_{m \in \mathcal{M}} |m|$.*

Given a bounded set $\mathcal{K} \subset \mathbb{Z}$, define the shifted uniform sampling sets X_k for $k \in \mathcal{K}$ by (4.0.4). If the number of elements in $\mathcal{K}$ is equal to the number of elements in $\mathcal{M}$, then the function f^ϵ can be uniquely reconstructed from the samples $f^\epsilon(z)$, $z \in \cup_k X_k$. Moreover, there is a positive constant $C = C(\delta x/\epsilon)$ such

that the following stability estimate holds

$$\|f^\epsilon\|_{L^2}^2 \leq C \sum_{y \in \cup_k X_k} |f^\epsilon(y)|^2. \tag{4.0.5}$$

The sampling strategy in the theorem above, illustrated in Figure 4.1, is very well matched with the grids used in multiscale methods. As an example, HMM provides a framework for capturing large scale features on coarse grids by incorporating local simulations on grids with much finer resolution, see [1, 32] and §4.1.

In the next section, we give a brief background to relevant issues in multiscale computation and information theory.

4.1 Multiscale representations in theory and computation

The goal of this work is to make a connection between computational grid practice in multiscale modeling and information theory, and to formulate sampling strategies for a class of continuous signals that includes cases where the sampling rate may result in aliasing.

Representation of multiscale functions

Fourier analysis is a standard way of representing signals $g \in L^2(\mathbb{R}^d)$ in terms of components on different scales. This representation extends to more general decompositions of signals in terms of a sequence $\{\phi_n\}_{n\in\mathbb{Z}} \subset L^2(\mathbb{R}^d)$

$$g(x) = \sum_{n=-\infty}^{\infty} \langle g, \phi_n \rangle \phi_n(x) \tag{4.1.1}$$

where $\langle \cdot, \cdot \rangle$ defines an inner product on the space. The vectors $\{\phi_n\}$ can form an orthonormal basis of, for example, trigonometric functions or wavelets.

Here we connect the two: starting with a bandlimited function $f(x, y)$ that has Fourier decomposition (4.1.1) given by

$$f(x, y) = \sum_{n=-\infty}^{\infty} f_n(x)\phi_n(y),$$

and then including a "fast" variable through the transformation $y \to x/\epsilon$. The resulting functions f^ϵ given by (4.0.1) have a multiscale representation in the viewpoints of both Fourier analysis and periodic homogenization.

Multiscale computation

Classical results from information theory are often cited as motivation for selecting the mesh size in the numerical analysis of a linear or nonlinear system that is discretized on a uniform grid $X = \{x_j \mid 0 \leq j \leq N\}$ with spacing $\Delta x = x_j - x_{j-1}$. In order to ensure that the solution to the discretized problem, $\{u_j\}_{j=0}^N$, is consistent with the solution to the true problem and the approximation is stable, the grid X must be sufficiently dense.

In order to approximate u^ϵ, the solution of a multiscale system, the uniform grid spacing Δx is chosen to be much smaller than the smallest scale in order to fully resolve the ϵ-scale. Multiscale algorithms exist that achieve a close approximation to u^ϵ on much coarser grids. They do this by exploiting the special properties of u^ϵ such as periodicity, scale separation, and bounded spectral support.

For example, in [1, 36] HMM is used for the solution of stiff ordinary differential equations (ODEs) of the form

$$\begin{cases} \frac{du^\epsilon}{dt} & = f(u^\epsilon, v^\epsilon, t), \\ \frac{dv^\epsilon}{dt} & = \frac{1}{\epsilon} g(u^\epsilon, v^\epsilon, t), \end{cases} \tag{4.1.2}$$

where v^ϵ is a solution that oscillates on the time scale of $O(\epsilon)$, $0 < \epsilon \ll 1$, and u^ϵ has variations mainly on the $O(1)$ time scale.

Assume that as $\epsilon \to 0$, $u^\epsilon \to U \in C^1(\mathbb{R})$ and that U is given by

$$\frac{d}{dt} U = \bar{f}(U, t). \tag{4.1.3}$$

This "effective" system can be solved using HMM even if the form of $\bar{f}$ is not explicitly known. The right hand side of (4.1.3) can be approximated using averaged solutions to the full system.

Figure 4.2 represents an HMM-type scheme for approximating the solution U of (4.1.3). The top directed axis represents the coarse grid that holds values of U. In the lower axis, local solutions u^ϵ, v^ϵ to (4.1.2) are computed using an initial condition determined by $U(t_n)$. Then, $\bar{f}$ is evaluated by averaging the solutions with a compactly supported kernel. This procedure is summarized below.

1. Reconstruction: at $T = t_n$ set the initial conditions for $u_n^\epsilon, v_n^\epsilon$ using U^n.

2. Microscale evolution: solve (4.1.2) in a local domain $t \in [t_n, t_{n+\eta}]$ and use an averaging kernel K to compute $\bar{f}(t_n) \sim \tilde{f}(t_n) = K * f^\epsilon(u_n^\epsilon, v_n^\epsilon)$.

Figure 4.2: **HMM for ordinary differential equations.** The diagram represents the macro-micro coupling in an HMM scheme for ODEs. Here, the solution is calculated on a local microscopic mesh in order to approximate the solution on the macroscopic grid.

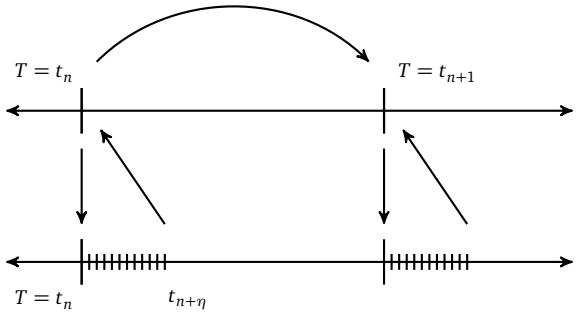

3. Macroscale evolution: compute U^{n+1} at $T = t_{n+1}$ using the values $\{U^j\}_{j=0}^n$ and $\{\tilde{f}(t_j)\}_{j=0}^n$.

Consider the following simple example of the type studied in [36],

$$\begin{cases} \frac{dx}{dt} = y^2, & x(0) = 0 \\ \frac{dy}{dt} = \frac{1}{\epsilon} z, & y(0) = 1 \\ \frac{dz}{dt} = \frac{1}{\epsilon} y, & z(0) = 0. \end{cases} \tag{4.1.4}$$

The solutions are $x(t) = \frac{t}{2} + \frac{\epsilon}{4}\sin(\frac{2t}{\epsilon})$, $y = \cos(\frac{t}{\epsilon})$, and $z(t) = \sin\frac{t}{\epsilon}$. The slow variable $x(t)$ is of the form given in (4.0.3).

Nonuniform discretizations are also used in approximation schemes for partial differential equations (PDEs), for example,

$$\begin{cases} -\nabla \cdot (a^\epsilon(x)\nabla u^\epsilon(x)) = f(x) & x \in \Omega \subset \mathbb{R}^d, \\ u^\epsilon(x) = 0, & x \in \partial\Omega. \end{cases} \tag{4.1.5}$$

Here, ϵ is a parameter satisfying $0 < \epsilon \ll 1$ that represents the ratio between the large and small scales in the multiscale coefficient $a^\epsilon(x) := a(x, x/\epsilon)$, where $a(x, y)$ is assumed to be periodic in y.

For $a^\epsilon \in L^\infty(\mathbb{R}^d)$ the solution u^ϵ of (4.1.5) contains a high frequency component of $\mathcal{O}(\epsilon^{-1})$ and a low frequency component of $\mathcal{O}(1)$. The problem (4.1.5) is well studied in homogenization theory [4, 15, 51, 69], and it demonstrates the application of these homogenization techniques in multiscale computation.

Numerical methods such as the finite element heterogeneous multiscale method [1, 32] approximate the solution to an effective problem using grids with macroscale spacing $\Delta x > \epsilon$.

The functions involved in homogenization theory and multiscale computation are often of lower regularity. In order to connect to information theory, we will approximate them by bandlimited functions. The rich theory of sampling for bandlimited functions, summarized in the next section, will aid us in the design of a suitable discretization.

Classical sampling theory for bandlimited signals

In 1765, Lagrange proved that periodic functions with trigonometric series expansions can be expressed as a linear combination of n sine and n cosine terms. In addition, he proved that such functions can be uniquely reconstructed from $2n + 1$ uniform samples of the function taken within a period. In 1841, Cauchy proved an interpolation formula for periodic functions with

limited wave-number using Lagrange interpolation in the proof [21].

Theorem 4.1.1 (Cauchy, 1841). *Let*

$$f(t) = \sum_{|n|\leq M} c_n e^{2\pi i t n} \tag{4.1.6}$$

and set $N = 2M + 1$. *Then,*

$$f(t) = \sin(\pi t N) \sum_{m=0}^{N-1} \frac{1}{N} f\left(\frac{m}{N}\right) \frac{(-1)^m}{\sin \pi(t - \frac{m}{N})}.$$

Theorem 4.1.1 is a sampling theorem that allows us to express f in terms of its samples $\{f\left(\frac{m}{N}\right)\}_{m=0}^{N-1}$. The functions that satisfy (4.1.6) belong to a broader class of functions that have a bounded spectrum, called *bandlimited functions*.

Definition 4.1.1. Let $\mathcal{F} \subset \mathbb{R}^d$ be a bounded set. The set of $\mathcal{F}$—bandlimited functions is denoted

$$\mathcal{B}(\mathcal{F}) = \{g \in L^2(\mathbb{R}^d) \mid \hat{g}(\xi) = 0 \text{ for all } \xi \notin \mathcal{F}\}.$$

If $f \in \mathcal{B}(\mathcal{F})$, we refer to f as a bandlimited or, more precisely, $\mathcal{F}$—bandlimited function.

The celebrated sampling theorem that Shannon used in his theory of communication, see [77, 76], provides a characterization of one-dimensional bandlimited signals.

Theorem 4.1.2 (Shannon Sampling Theorem). *If a function* $f \in L^2(\mathbb{R})$ *contains no frequencies higher than* W *cycles per second it is completely determined by giving its ordinates at a series of points spaced* $(1/2W)$ *s apart.*

Though Shannon is credited with introducing this theorem to information theory, he was aware that the result was widely known in communication theory [66]. Equivalent theorems existed in the mathematical literature, including the work of both E.M. and J.T. Whittaker [91, 92, 93] and Kotel'nikov [55].

We shall now state the Classical Sampling Theorem adapted to our mathematical framework.

Theorem 4.1.3 (Classical Sampling Theorem). *Let $W > 0$ and choose Δx to be a fixed constant that satisfies $0 < 2W\Delta x \leq 1$. Then*

$$\forall f \in \mathcal{B}([-W, W]), \quad f(x) = \sum_{n=-\infty}^{\infty} f(n\Delta x) \frac{\sin \pi(x - n\Delta x)}{\pi(x - n\Delta x)}, \tag{4.1.7}$$

where the convergence of the sum is in the L^2—norm and uniformly on $\mathbb{R}$.

The set $\{n\Delta x\}_{n\in\mathbb{Z}}$ in (4.1.7) is called a *uniform sampling set* because it consists of equidistant sampling points with spacing Δx. The *sampling rate* is the number of samples taken per second. Theorem 4.1.3 states that a sampling rate $\frac{1}{\Delta x} \geq 2W$ is needed in order to guarantee the unique reconstruction of a $[-W, W]$—bandlimited function from its uniform samples. The minimum sampling rate of $2W$ is known as the *Nyquist rate*.

Uniform sampling theory has been developed in more general contexts, including sampling of bandpass signals $f \in \mathcal{B}([-W + W_0, W + W_0])$ [54], the d—dimensional uniform sampling theorem of Middleton and Peterson [71], and the sampling theorem for locally compact abelian groups [53].

Nonuniform sampling theory

In this work, we are interested in sampling signals that arise in important applications, including image processing, geophysics, and optical tomography. Due to the nature of the acquisition of measurements, it is not always possible to sample a function uniformly. Therefore, it is important to study the theory of *nonuniform* or *irregular* sampling.

Irregular sampling involves the reconstruction of a bandlimited function from nonuniformly spaced samples. For a review of the nonuniform sampling literature, see [62], and for theoretical and numerical aspects of nonuniform sampling, see [14, 40, 46]. An example is multivariate sampling, where Shannon's theory is extended to the recovery of signals from the responses of m linear shift-invariant systems sampled at $1/m$ times the reconstruction rate [68]. Sampling in this way allows us to use prior knowledge of the representation of a signal to design a sampling strategy that simplifies the reconstruction process.

An example of multivariate sampling of interest is *periodic nonuniform sampling*, where the sampling set is the collection of sampling sets of the form $\{j\Delta x + k\delta x \mid j \in \mathbb{Z}^d\}$ for k in $\mathbb{Z}^d$. This type of sampling is well studied in the signal processing literature [59, 74, 87, 90, 95]. One major challenge in the design of nonuniform sampling strategies from a practical point of view is the stability of the reconstruction [60].

Definition 4.1.2. Let $\mathcal{F} \subset \mathbb{R}$ be a bounded set. For a given sampling strategy, a sampling set $X = \{x_j\}$ is a *set of stable sampling* for $\mathcal{B}(\mathcal{F})$ if there exists a constant

$C > 0$ such that

$$\int_{-\infty}^{\infty} |g(x)|^2 dx \leq C \sum_j |g(x_j)|^2 \text{ for all } g \in \mathcal{B}(\mathcal{F}).$$

Uniqueness and stability results for the nonuniform sampling of bandlimited functions are provided by Beurling and Landau [16, 58, 57]. In these works, a bound is obtained on the minimum sampling density required for the stable reconstruction of a bandlimited function. This density, called the *Beurling-Landau density* is determined by the sum of the bandwidths of a function. For multiband functions with large spectral gaps, the Beurling-Landau density allows for stable sampling at a rate that is much lower than the Nyquist rate. The main result in this paper produces a stable set of sampling for a class of multiscale functions with a sampling density that attains the Landau bound.

There is an enormous volume of literature on sampling theory and its various generalizations and extensions [13, 50, 61, 67, 68, 86, 88]. Irregular sampling of bandlimited functions has been extensively studied in the context of frame theory of [30] that motivated the development of iterative methods for reconstruction using the frame-method [14, 40, 39, 94]. There are very similar nonuniform sampling theorems using bunched samples to reconstruct functions that have spectral gaps [12, 68, 87, 89]. The result presented here differs from these results in terms of conditions on the spectral gaps or the notion of stability.

4.2 Spectral properties of bandlimited multiscale functions

This section describes properties of functions that are studied in multiscale analysis. We begin with an example from [34] of basic multiscale functions in one dimension that satisfy (4.0.1), and derive the spectral property (4.0.3).

Example 2 ($d = 1$)**.** Consider functions with scaling law representation

$$f^\epsilon(x) = f(x, x/\epsilon)$$

where $f(x,y)$ is $(\Omega \times \mathcal{M})$—bandlimited and 1-periodic in *both* variables. The spectrum of f is therefore supported in the discrete set $\Omega \times \mathcal{M}$, where $\Omega = \{0, 1, \dots N\}$ and $\mathcal{M} = \{0, 1, \dots M\}$. These assumptions allow for the representation of $f(x,y)$ by a finite Fourier series:

$$f(x,y) = \sum_{n=0}^{N} \sum_{m=0}^{M} f_{n,m} e^{2\pi i(nx+my)}. \tag{4.2.1}$$

The multiscale function $\hat{f}^\epsilon$ has Fourier transform

$$\hat{f^\epsilon}(k) = \sum_{n=0}^{N} \sum_{m=0}^{M} f_{n,m} \delta(k - n - \frac{m}{\epsilon}),$$

where $\delta(x)$ is the Dirac delta function. Then, the support of the spectrum of $\hat{f}$ can be computed,

$$\hat{f}^\epsilon(k) = 0, \quad k \notin \bigcup_{m \in \mathcal{M}} \left(\Omega + \frac{m}{\epsilon}\right).$$

Now, removing the assumption that $f(x,y)$ is periodic in x, tools from Fourier analysis can be applied to construct multiscale functions from locally

periodic functions of two variables. This construction will allow us to derive the spectral property (4.0.3).

The next lemma provides the specific structure of the spectrum of bandlimited multiscale functions.

Lemma 4.2.1. *The Fourier transform of $f^\epsilon \in L^2(\mathbb{R}^d)$ defined by (4.0.1) − (4.0.2) satisfies*

$$\hat{f}^\epsilon(\xi) = 0, \quad \xi \notin \bigcup_{m\in\mathcal{M}} \left(\Omega + \frac{m}{\epsilon}\right).$$

Proof. Set $Y = \mathbb{T}^d$. For every fixed $x \in \mathbb{R}^d$, the Fourier series expansion of $f(x,y)$ has the form

$$f(x,y) = \sum_{m\in\mathcal{M}} c_m(x)\, e^{2\pi i\langle m,y\rangle}; \quad c_m(x) = \int_Y f(x,y)\, e^{-2\pi i\langle m,y\rangle} dy. \tag{4.2.2}$$

It is readily seen that the Fourier coefficients $c_m(x)$ lie in the space $\mathcal{B}(\Omega)$ by taking the Fourier transform,

$$\begin{aligned}
\hat{c}_m(\xi) &= \int_{\mathbb{R}^d} \left(\int_Y f(x,y)\, e^{-2\pi i\langle m,y\rangle} dy \right) e^{-2\pi i\langle \xi,x\rangle} dx \\
&= \int_Y \int_{\mathbb{R}^d} f(x,y)\, e^{-2\pi i(\langle m,y\rangle + \langle \xi,x\rangle)} dx dy \\
&= \hat{f}(\xi, m) = 0 \text{ for all } \xi \notin \Omega.
\end{aligned}$$

Substituting $\left(x, \frac{x}{\epsilon}\right)$ for (x,y) in (4.2.2) results in the representation

$$f^\epsilon(x) = \sum_{m\in\mathcal{M}} c_m(x)\, e^{2\pi i\langle m,x/\epsilon\rangle}; \qquad c_m \in \mathcal{B}(\Omega). \tag{4.2.3}$$

For $\xi \in \mathbb{R}^d$, the Fourier transform $\hat{f}(\xi)$ can be expressed as

$$\hat{f^\epsilon}(\xi) = \sum_{m \in \mathcal{M}} \hat{c}_m \Big(\xi - \frac{m}{\epsilon} \Big),$$

and since $\hat{c}_m(\xi - \frac{m}{\epsilon}) = 0$ for $\xi \notin \Omega + \frac{m}{\epsilon}$, it follows that

$$\hat{f}^\epsilon(\xi) = 0, \quad \xi \notin \bigcup_{m \in \mathcal{M}} \Big(\Omega + \frac{m}{\epsilon} \Big).$$

□

The special structure of the spectral support of multiscale functions given by Lemma 4.2.1 will allow for the design of nonuniform sampling schemes as in [34]. Our aim is to find a sampling scheme that is *sub-Nyquist*, that is, if W is the intersection of connected sets containing the support of $\hat{f}^\epsilon$, we will design stable sampling sets for $\hat{f}^\epsilon$ that have spacing $\Delta x > \frac{1}{|W|}$.

4.3 Nonuniform sampling strategy

For the sampling sets X_k defined by (4.0.4), the aim is to derive sufficient conditions on Δx and δx so that the function f^ϵ can be uniquely and stably recovered from the nonuniform samples $f^\epsilon(z)$, $z \in \cup_k X_k$. In general, when sampling at a sub-Nyquist rate, the unique recovery of f^ϵ is not guaranteed. We can, however, describe the function reconstructed from undersampling.

Example 3. Let $f^\epsilon(x)$ be a function defined in Example 2 and assume, for simplicity, that $\epsilon = 1/L_1$ for a positive integer L_1. According to Theorem 4.1.3, the stable reconstruction of f^ϵ from uniform samples requires a sampling rate of $O(\epsilon^{-1})$.

In the nonuniform sampling set used in [34], the sampling points $\{x_{j,k}\}$ are clustered in groups with $\Delta x = 1/L_2$, for L_2, L_1/L_2 positive integers,

$$x_{j,k} = j\Delta x + k\delta x \qquad 1 \le j \le J, \quad 1 \le k \le K \quad (\delta x \ll \Delta x).$$

Evaluating the expression (4.2.1) at each sampling point results in a system of equations

$$\sum_{n=0}^{N}\sum_{m=0}^{M} f_{n,m} e^{2\pi i(nx_{j,k}+mx_{j,k}/\epsilon)} = f^{\epsilon}(x_{j,k}).$$

This system is invertible when $J > N$ and $K > M$ and the conditions $\delta x < \epsilon/M$ and $\Delta x < 1/N$ are satisfied. This shows that it is possible to take advantage of the special structure of f^{ϵ} and uniquely reconstruct the function from samples taken from nonuniform sampling set with $O(N)$ density.

In the following we assume that $f^{\epsilon} \in L^2(\mathbb{R}^d)$ defined by (4.0.1) – (4.0.2). In this case, $f^{\epsilon} \in \mathcal{B}\left(\cup_{m\in\mathcal{M}}(\Omega + \frac{m}{\epsilon})\right)$. The proof involves a modification of arguments from [12] that assume that the uniform sampling lattices have spacing Δx that is an integer multiple of ϵ. Instead, we will prove results using vectors L_m and α_m, where $(L_m)_i$ are integers and $(\alpha_m)_i \in [0, 1/\Delta x)$ are the unique constants that satisfy

$$\frac{m}{\epsilon} = \frac{L_m}{\Delta x} + \alpha_m.$$

For these more general classes of functions and sampling sets, a sampling operator is needed that constructs functions using a Shannon-type reconstruction formula from uniform samples taken at sub-Nyquist sampling rate.

Lemma 4.3.1. *For a bounded set $\Omega \subset \mathbb{R}^d$ and a multiscale function $g(x)$ satisfying the assumptions of Lemma 4.2.1, the function $S_{X_k} g(x)$ corresponding to the sampling set*

$$X_k = \{j\Delta x + k\delta x \mid j \in \mathbb{Z}^d\}, \qquad \Delta x < \frac{1}{|\Omega|},$$

defined by the formula

$$S_{X_k} g(x) = \sum_{y \in X_k} g(y)\varphi_s(x-y), \qquad \varphi_s(z) = \frac{1}{|\Omega_s|}\int_{\Omega_s} e^{2\pi i\langle z,\xi\rangle} d\xi, \tag{4.3.1}$$

where $\Omega_s = [-\frac{1}{2\Delta x}, \frac{1}{2\Delta x}]^d$, is square-integrable and satisfies

$$S_{X_k} g(y) = g(y) \quad \text{for all } y \in X_k. \tag{4.3.2}$$

Proof. Due to (4.2.3), g has a representation

$$g(x) = \sum_{m \in \mathcal{M}} g_m(x) e^{2\pi i\langle m, x/\epsilon\rangle}, \qquad g_m \in \mathcal{B}(\Omega) \text{ for } m \in \mathcal{M}.$$

Applying the sampling operator to each g_m results in

$$\left(S_{X_k} g_m e^{2\pi i\langle m,\cdot/\epsilon\rangle}\right)(x) = \sum_{y \in X_k} g_m(y) e^{2\pi i\langle m,y\rangle/\epsilon}\varphi_s(x-y). \tag{4.3.3}$$

The function defined by $\tilde{g}_m = g_m(x + k\delta x)$ also lies in the space $\mathcal{B}(\Omega)$, and we can bound the magnitude of the terms in the sum (4.3.3) by

$$\begin{aligned}\sum_{y \in X_k} |g_m(y) e^{2\pi i\langle m/\epsilon, y\rangle}\varphi_s(x-y)| &= \sum_{y \in X_0} |g_m(y + k\delta x) e^{2\pi i\langle m/\epsilon, y+k\delta x\rangle}\varphi_s(x-y-k\delta x)| \\ &\le \left(\sum_{y \in X_0} |\tilde{g}_m(y)|^2\right)^{1/2} < \infty.\end{aligned}$$

The last statement holds because of the Cauchy Schwartz inequality and the square integrability of $\tilde{g}_m$. Therefore the series (4.3.3) is uniformly absolutely-convergent and

$$\|S_{X_k} g_m e^{2\pi i\langle m,\cdot/\epsilon\rangle}\|^2_{L^2(\Omega)} \leq \left(\sum_{y\in X_0} |\tilde{g}_m(y)|^2\right) \|\varphi_s\|^2_{L^2(\Omega)} < \infty.$$

Summing over m in the set $\mathcal{M}$,

$$\begin{aligned}\sum_{m\in\mathcal{M}} \left(S_{X_k} g_m e^{2\pi i\langle m,\cdot/\epsilon\rangle}\right)(x) &= \sum_{m\in\mathcal{M}} \sum_{y\in X_k} g_m(y) e^{2\pi i\langle m,y\rangle/\epsilon} \varphi_s(x-y) \\ &= \sum_{y\in X_k} \sum_{m\in\mathcal{M}} g_m(y) e^{2\pi i\langle m,y\rangle/\epsilon} \varphi_s(x-y) \\ &= \sum_{y\in X_k} g(y)\varphi_s(x-y) = S_{X_k} g(x).\end{aligned}$$

Since $\mathcal{M}$ is a finite set, the function $S_{X_k} g(x)$ is a finite sum of square-integrable functions, and is therefore also square-integrable.

Also, we can show that $\varphi_s(0) = 1$ and $\varphi_s(y) = 0$ for $y \in X_0$, $y \neq 0$. Let $y = n\Delta x$, $n \neq 0$.

$$\begin{aligned}\varphi_s(0) &= \frac{1}{|\Omega_s|} \int_{\Omega_s} d\xi = 1, \\ \varphi_s(y) &= \frac{1}{|\Omega_s|} \int_{\Omega_s} e^{2\pi i\langle n\Delta x,\xi\rangle} d\xi, \\ &= \int_{[\frac{-1}{2},\frac{1}{2}]^d} e^{2\pi i\langle n,\xi'\rangle} d\xi' = 0.\end{aligned}$$

Therefore, we have shown that (4.3.2) holds.

□

The next lemma provides the explicit form of the function reconstructed from sub-Nyquist sampling of f^ϵ.

Lemma 4.3.2. *Let f^ϵ satisfy (4.2.3). The function $S_{X_k} f^\epsilon$ defined by (4.3.1) is square integrable and has the explicit form*

$$S_{X_k} f^\epsilon(x) = \sum_{m \in \mathcal{M}} c_m(x) e^{2\pi i(\langle \alpha_m, x\rangle + \langle L_m/\Delta x, k\delta x\rangle)}. \tag{4.3.4}$$

Moreover, the reconstruction of $S_{X_k} f^\epsilon$ is stable,

$$\|S_{X_k} f^\epsilon\|^2_{L^2(\Omega)} < \frac{1}{|\Omega|} \sum_{y \in X_k} |f^\epsilon(y)|^2. \tag{4.3.5}$$

Proof. By Lemma 4.3.1, the function $S_{X_k} f^\epsilon$ is well defined and square-integrable. The sampled function can be expressed in terms of its sampled Fourier coefficients

$$S_{X_k} f^\epsilon(x) = \sum_{m \in \mathcal{M}} S_{X_k} c^\epsilon_m(x), \tag{4.3.6}$$

where $c^\epsilon_m(x) = c_m(x) e^{2\pi i \langle m/\epsilon, x\rangle}$ is a function in the space $\mathcal{B}\left(\Omega + \frac{m}{\epsilon}\right)$.

Define the shifted function $d_m(x) = c_m(x + k\delta x) e^{2\pi i \langle m/\epsilon, k\delta x\rangle}$. Then, for

each m in $\mathcal{M}$,

$$\begin{aligned}
S_{X_k} c_m^\epsilon(x) &= \sum_{y\in X_k} c_m(y) e^{2\pi i\langle m/\epsilon, y\rangle} \varphi_s(x-y) \\
&= \sum_{y\in X_0} d_m(y) e^{2\pi i\langle \alpha_m, y\rangle} \frac{1}{|\Omega_s|} \int_{\Omega_s} e^{2\pi i\langle x-y-k\delta x, \xi\rangle} d\xi \\
&= \int_{\Omega_s} \left[\frac{1}{|\Omega_s|} \sum_{y\in X_0} d_m(y) e^{-2\pi i\langle y, \xi-\alpha_m\rangle} \right] e^{2\pi i\langle x-k\delta x, \xi\rangle} d\xi \\
&= \int_{\Omega_s} \left[\sum_{z\in\Omega_s^{-1}} \hat{d}_m(\xi-\alpha_m+z) \right] e^{2\pi i\langle x-k\delta x, \xi\rangle} d\xi \qquad (4.3.7) \\
&= \int_{\Omega_s} \hat{d}_m(\xi-\alpha_m) e^{2\pi i\langle x-k\delta x, \xi\rangle} d\xi \\
&= d_m(x-k\delta x) e^{2\pi i\langle \alpha_m, x-k\delta x\rangle} \\
&= c_m(x) e^{2\pi i(\langle \alpha_m, x\rangle + \langle L_m/\Delta x, k\delta x\rangle)}. \qquad (4.3.8)
\end{aligned}$$

Here, the set $\Omega_s^{-1} = \{k/\Delta x \mid k \in \mathbb{Z}^d\}$ is called the *reciprocal lattice*.

Since the functions c_m and φ_s are both square integrable, the sums converge uniformly and the exchange between sum and integral is justified. The Poisson summation formula in $\mathbb{R}^d$ is used for (4.3.7) [72]. Then, substituting (4.3.8) in (4.3.6) proves the reconstruction formula. For stability,

$$\|S_{X_k} f^\epsilon\|_{L^2(\Omega)}^2 \le \frac{1}{|\Omega_s|} \sum_{y\in X_k} \| f^\epsilon(y)\varphi_s(\cdot - y)\|_{L^2(\Omega)}^2 < \frac{1}{|\Omega|} \sum_{y\in X_k} |f^\epsilon(y)|^2.$$

□

The expression (4.3.1) will be used in the proof of the main result.

Proof of Theorem 4.0.1

For simplicity, we set $\mathcal{M} = \{0, 1, \ldots, M\}$ and $\mathcal{K} = \{0, 1, \ldots, K\}$. The stable reconstruction formula for multiscale functions f^ϵ is proved using an approach similar to [34].

We will use a result from [45], concerning the estimation of the norm of the inverse of Vandermonde matrices.

Theorem 4.3.1 (Gautschi, 1990). *For arbitrary $w_l \in \mathbb{C}$, with $w_l \neq w_{l'}$ if $l \neq l'$, there holds*

$$\max_l \prod_{l' \neq l} \frac{\max(1, |w_{l'}|)}{|w_l - w_{l'}|} \leq \|V^{-1}\|_\infty \leq \max_l \prod_{l' \neq l} \frac{1 + |w_{l'}|}{|w_l - w_{l'}|}, \tag{4.3.9}$$

where V is a Vandermonde matrix with elements $w_0, \ldots w_M \in \mathbb{C}$. The upper bound is obtained if $w_l = |w_l| e^{i\theta}, l = 0 \ldots, M$ for some fixed $\theta \in \mathbb{R}$.

Proof. The set of equations from (4.3.4) form the linear system

$$S_{X_k} f^\epsilon(x) = \sum_{m \in \mathcal{M}} c_m^\alpha(x) e^{2\pi i \langle L_m/\Delta x, k\delta x \rangle}.$$

where $c_m^\alpha(x) = c_m(x) e^{2\pi i \langle \alpha_m, x \rangle}$. When $K = M$, the corresponding Vandermonde matrix V contains the elements $V_{mk} = w_m^k$ for $w_m = e^{2\pi i \frac{L_m}{\Delta x} \delta x}$. The requirement that $w_0, \ldots w_M$ are distinct elements results in an invertible system.

Since $0 < \frac{\delta x}{\epsilon} < \frac{1}{M+1}$, the elements $w_0, \ldots, w_M$ are distinct nodes distributed on the upper half plane of the unit circle. This ensures the existence of

V^{-1}. As a result, the reconstruction formula for f^ϵ is well defined:

$$f^\epsilon(x) = \sum_{j\in\mathcal{M}} c_j^\alpha(x) e^{2\pi i \frac{L_j}{\Delta x}x} \tag{4.3.10}$$

$$= \sum_{j\in\mathcal{M}} \left(\sum_{k\in\mathcal{K}} (V^{-1})_{jk} S_{X_k} f^\epsilon(x) \right) e^{2\pi i \frac{L_j}{\Delta x}x}. \tag{4.3.11}$$

Using some properties of Vandermonde matrices, and the result from Theorem 4.3.1, it can be shown that this formula is stable.

The upper bound on $|w_l - w_{l'}|$ can be computed

$$|w_l - w_{l'}| \le |e^{2\pi i M\delta x/\epsilon} - 1| < |e^{2\pi i \frac{M}{2M+1}} - 1| < 2. \tag{4.3.12}$$

Now we compute the smallest distance between adjacent nodes. In the first case, for $0 \le l < M$,

$$|w_{l+1} - w_l| = |e^{2\pi i(\frac{1}{\epsilon} - (\alpha_{l+1} - \alpha_l))\delta x} - 1| > |e^{2\pi i(\frac{1}{\epsilon} - \Delta x)\delta x} - 1|.$$

The distance between adjacent nodes w_0 and w_M satisfy

$$|w_0 - w_M| \ge |e^{2\pi i M\delta x/\epsilon} - 1| > |e^{2\pi i \delta x/\epsilon} - 1| > |e^{2\pi i(\frac{1}{\epsilon} - \Delta x)\delta x} - 1|.$$

Since $\Delta x < \frac{1}{\epsilon}$, the last term in both cases is nonzero. Then, we have the estimate

$$\frac{1}{2^{M+1}} < \|V^{-1}\|_\infty \le \frac{1}{|e^{2\pi i(\frac{1}{\epsilon} - \Delta x)\delta x} - 1|^{M+1}}.$$

A final stability estimate for the reconstruction of f^ϵ from sampling sets $X_k, k \in \mathcal{K}$ is

$$\begin{aligned} \|f^\epsilon\|_{L^2}^2 &\le \|V^{-1}\|_\infty \| \sum_{k\in\mathcal{K}} S_{X_k} f^\epsilon(x)\|_{L^2}^2 \\ &< C(\delta x/\epsilon) \sum_{y\in\cup_k X_k} |f^\epsilon(y)|^2, \end{aligned}$$

where $C(\delta x/\epsilon) = \frac{M+1}{|\Omega|}\left(|e^{2\pi i(\frac{1}{\epsilon}-\Delta x)\delta x}-1|^{-(M+1)}\right)$. □

4.4 Some extensions and generalizations

Localized microscale

Multiscale models can be divided into different groups based on common features of the problems. In [1, 32], type A problems are described as problems that require microscale resolution with a microscale solver in a fixed number of local domains. This could be in order to resolve isolated defects such as dislocations, cracks, shocks, and contact lines. Outside of these local domains, the macroscale solver is used. Type B problems require some microscale information throughout the entire computational domain. Localized microscale simulations are used to supply missing information to the microscale solver.

The sampling analysis in the earlier sections have referred to type B problems. There are also links to information theory for type A problems involving functions of the following form

$$\lim_{|t|\to\infty} f(t) = \begin{cases} f_+(t), & t > 0 \\ f_-(t), & t < 0, \end{cases} \tag{4.4.1}$$

where f^+, f^- are branches of bandlimited function. We will assume the specific form $f(\gamma_\epsilon^{-1}(t))$, where the transformation γ_ϵ models the behavior of the isolated defect. Adaptive mesh refinement techniques are designed for these problems to provide higher resolution near a singularity or a domain of strong variation. These types of discretizations match well with the sampling results in [24, 52] for time warped signals.

In [24], the exact reconstruction of f from irregularly spaced samples $\{t_n\}$ is guaranteed, provided that there exists a continuous, injective mapping $t_n \to \gamma(t_n)$. The main result for time warped one dimensional signals is the following theorem.

Theorem 4.4.1 (Clark, 1985). *Let a function $f(t)$ of one variable be sampled at the points $t = t_n, n \in \mathbb{Z}$, where t_n is not necessarily a sequence of uniformly spaced numbers. If a 1-1 continuous mapping $\gamma(t)$ exists such that $n/2W = \gamma(t_n)$, and if $h(\tau) = f(\gamma^{-1}(\tau))$ is bandlimited to $[-W, W]$, then the following equation holds*

$$f(t) = \sum_{n=-\infty}^{\infty} f(t_n) \frac{\sin(2W\gamma(t) - n)}{2W\gamma(t) - n}. \tag{4.4.2}$$

As an example, we set $f^{\epsilon}(t) = \sin(t + 2\arctan(t/\epsilon))$. Then, $f_+(t) = \sin(t + \pi)$ and $f_-(t) = \sin(t - \pi)$. Define $\gamma_{\epsilon}^{-1} : \mathbb{R} \to \mathbb{R}$ by the transformation

$$\gamma_{\epsilon}^{-1}(t) = t + \arctan(t/\epsilon).$$

Since γ_{ϵ}^{-1} is surjective and $(\gamma_{\epsilon}^{-1})'(t) = 1 + \frac{\epsilon^{-1}}{\sqrt{1+(t\epsilon^{-1})^2}} > 0$, it follows that $\gamma_{\epsilon}(t) := (\gamma_{\epsilon}^{-1})^{-1}(t)$ is well defined.

Then, there exists a set of sampling points $t_n, n \in \mathbb{Z}$ such that $\gamma_{\epsilon}(t_n) = n$. The function $h(\tau) = f(\gamma_{\epsilon}(\tau))$ is a bandlimited function that can be reconstructed from the uniform samples at points $\tau_n = \gamma_{\epsilon}(t_n)$. Therefore, the original function can recovered using the relation $f(t) = h(\gamma_{\epsilon}^{-1}(t))$, and we have shown that recovery of f is possible using the nonuniform sampling set $\gamma_{\epsilon}(t_n), n \in \mathbb{Z}$.

There are cases where the explicit form of the transformation γ is unknown. In [52], a local estimate $B(t)$ of the effective bandwidth of f is made

using techniques such as the windowed Fourier transform. A disadvantage here is that the "local" bandwidth cannot be extended globally.

We have that a signal with time varying bandwidth $B(t)$ can be defined as

$$f(t) = \sin(2\pi\phi(t)),$$

where the phase function $\phi(t)$ is defined in terms of the instantaneous signal frequency by $\phi'(t) = B(t)$. The samples required for an exact reconstruction are given implicitly

$$t_n = n/(2B(t_n)).$$

In the above example, this corresponds to a sampling set of the form

$$t_n = \frac{n\pi}{t_n + 2\arctan(t_n/\epsilon)}.$$

Sampling in higher dimensions

The uniform sampling theorem in higher dimensions is described in [71], along with an optimal sampling rate. We set basis vectors $v_1, v_2 \in \mathbb{R}^d$, $v_1 \neq kv_2$, determined by points on the sampling set

$$x_{[l]} = l_1 v_1 + \ldots + l_d v_d, \qquad l_i = 0, \pm 1, \pm 2, \ldots \tag{4.4.3}$$

An example of (4.4.3) for $d = 2$ is a rectangular grid, where $v_1 = (\Delta x, 0), v_2 = (0, \Delta x)$.

We will now state the higher dimensional sampling theory of Peterson and Middleton [71].

Theorem 4.4.2 (Sampling theorem in d dimensions, Peterson, Middleton, 1962). *A function $f(x)$ whose Fourier transform $\hat{f}$ vanishes over all but a finite portion of wave-number space can be everywhere reproduced from its sampled values taken at a lattice of points $\{l_1 v_1 + \ldots l_d v_d\}$, $l_i = 0, \pm 1, \pm 2, \ldots$, provided that the vectors $\{v_j\}$ are small enough to ensure nonoverlapping of the spectrum $\hat{f}$ with its images on a periodic lattice defined by the vectors $\{u_j\}$ with $\langle v_j, u_k \rangle = 2\pi\delta_{jk}$.*

Extensions of the one-dimensional irregular sampling theory are provided in [38], for functions that are bandlimited to the set $\Omega = [-\omega_1, \omega_1] \times [-\omega_2, \omega_2]$. Reconstruction in these cases require assumptions about the product structure of the sampling sets or the use of algorithms that are known to converge [46]. For $d \geq 2$, irregular sampling theorems are given that require a sampling density equal to the Nyquist density in [40, 47]. Numerical algorithms for irregular sampling are given in [81].

The theory for sub-Nyquist sampling of *multiband* functions in higher dimensions is incomplete (to the best knowledge of the author). The case $d = 2$ for discrete-time signals is considered in [87]. In [12], a generalized sampling theory for locally compact abelian groups is developed under assumptions on the structure of the sampling sets.

The results in §4.3 allow us to adapt Theorem 4.0.1 for $d \geq 1$.

Corollary 4.4.1. *Let $f^\epsilon(x)$ satisfy (4.0.1) − (4.0.3) for a discrete set of frequencies $\mathcal{M} = \{m_1, \dots, m_P\}$. Then, f^ϵ can be recovered uniquely from samples on the set $\{j\Delta x + k\delta x, \mid j, k \in \mathbb{Z}^d, k = k_1, \dots k_Q\}$ if the matrix V with entries*

$$V_{mk} = e^{2\pi i \langle k\delta x, L_m/\Delta x\rangle}$$

is invertible. In particular, necessary conditions are $Q \geq P$.

Proof. Lemma 4.3.2 provides the solution of the system of equations

$$S_{X_k} f^\epsilon(x) = \sum_{m\in\mathcal{M}} c_m(x) e^{2\pi i(\langle \alpha_m, x\rangle + \langle k\delta x, L_m/\Delta x\rangle)}. \tag{4.4.4}$$

Invertibility of the system allows for the recovery of the shifted Fourier components $c_{m_1}(x)e^{2\pi i\langle \alpha_{m_1}, x\rangle}, \dots, c_{m_p}(x)e^{2\pi i\langle \alpha_{mp}, x\rangle}$. Multiplying each c_m by a factor of $e^{2\pi i\langle L_m, \Delta x\rangle}$ recovers the m^{th} frequency component of f^ϵ, and summing over all m gives the result. □

In the case of $d = 1$, we showed sufficient conditions on the sampling sets that resulted in an invertible Vandermonde matrix V. In higher dimensions, the fundamental theorem of algebra does not hold and the invertibility of the system is not guaranteed. In [12], it is shown that stable recovery is possible through iterative reconstruction when the sampling sets follow certain admissibility conditions.

Chapter 5

Numerical methods for multiscale inverse problems

Inverse problems for partial differential equations pose a huge computational challenge, in particular when the coefficients are of multiscale form. An application is medical imaging, where high resolution reconstructions are obtained using photo-acoustic effects of optical and ultrasonic waves [10, 11]. We also consider examples in reflection seismology [82], where accurate models of seismic wave propagation in the Earth's sedimentary crust must account for a wide spectrum of time and spatial scales. The mathematical formulation is as follows.

For a bounded, connected domain, $\Omega \subset \mathbb{R}^d$, we will consider the problem

$$-\nabla \cdot (a^\epsilon \nabla u^\epsilon) + b^\epsilon u^\epsilon = f \text{ in } \Omega. \tag{5.0.1}$$

Here, $f \in H^{-1}(\Omega)$, $b^\epsilon \in L^\infty(\Omega)$, and a^ϵ is a symmetric, uniformly positive definite matrix function with bounded elements. The constant $0 < \epsilon \ll 1$ represents the ratio of scales in the problem. When faced with balancing computational cost with accuracy, most approaches only deal with scientific models of large scale behavior and, for example, account for microscopic processes by using effective or homogenized equations to simplify computations.

Homogenization theory [15, 51] provides the form of the effective problem corresponding to the family of functions $u^\epsilon \in H_0^1(\Omega)$ that satisfy (5.0.1); as $\epsilon \to 0$, the solutions converge weakly, $u^\epsilon \rightharpoonup U$ in $H_0^1(\Omega)$, where U is the solution to an equation of the form

$$-\nabla \cdot (A\nabla U) + \overline{b}U = f \text{ in } \Omega. \tag{5.0.2}$$

Here, A and $\overline{b}$ are called the *effective* or *homogenized coefficients* corresponding to a^ϵ and b^ϵ respectively.

5.1 Inversion using PDE-constrained optimization

In the abstract framework, the inverse problem is to determine an unknown parameter $a \in X$ where a is typically a function lying in the Banach space X. The given data is denoted $d_* \in Y$, where Y is also a Banach space; typically $Y = \mathbb{R}^M$. The *observation operator* $\mathcal{G} : X \to Y$ is the forward mapping from the unknown parameter to the data, and the *prediction operator* $\mathcal{F} : X \to Y$ is the forward mapping from the unknown parameter to the prediction.

In our context of multiscale inverse coefficient problems for PDEs, $\mathcal{G}$ maps the unknown parameter $a^\epsilon \in X$ to $\mathcal{G}(u^\epsilon, \nabla u^\epsilon, x) \in Y$, where u^ϵ solves the PDE (5.0.1), denoted by the state equation

$$c(a^\epsilon, u^\epsilon) = 0.$$

The prediction operator $\mathcal{F}$ maps an unknown macroscopic parameter A to the function $\mathcal{G}^0(U, \nabla U, x) \in Y$, where U solves the homogenized PDE (5.0.2), de-

noted by the state equation

$$c^0(A,U)=0.$$

The functions $\mathcal{G}$ and $\mathcal{G}^0$ measure properties of the solution and its gradient taken on the full domain or part of the domain, for example, on the boundary.

A common approach is to formulate the full inverse problem as a PDE-constrained optimization problem of the form

$$\begin{aligned} \underset{a^\epsilon,u^\epsilon}{\text{minimize}} \quad & \mathcal{J}(a^\epsilon,u^\epsilon) := \frac{1}{2}\|\mathcal{G}(u^\epsilon,\nabla u^\epsilon,x)-d_*\|^2+\alpha\mathcal{R}(a^\epsilon) \\ \text{subject to} \quad & c(a^\epsilon,u^\epsilon)=0. \end{aligned} \tag{5.1.1}$$

The constraint $c(a^\epsilon,u^\epsilon)=0$ is satisfied when u^ϵ solves the state equation (5.0.1).

Full inversion has a high computational cost and is typically ill-posed; a number of different sequences a^ϵ give the same homogenized solution U, $\lim_{\epsilon\to 0} u^\epsilon = U$. In [70], the full inverse problem (5.1.1) is replaced with an effective inverse problem, formulated as

$$\begin{aligned} \underset{A,U}{\text{minimize}} \quad & \mathcal{J}^0(A,U) := \frac{1}{2}\|\mathcal{G}^0(U,\nabla U,x)-d_*\|^2+\alpha\mathcal{R}(A) \\ \text{subject to} \quad & c^0(A,U)=0, \end{aligned} \tag{5.1.2}$$

where the constraint $c^0(A,U)=0$ is satisfied when U solves the effective state equation (5.0.2).

This paper explores the possibility of explicitly including the microscale components of the forward model in the inversion process by assuming a priori knowledge of the microstructure in the form of a low dimensional parametrization. This is achieved by imposing the additional constraint

$$a^\epsilon(x)=a(x/\epsilon,m(x)),$$

where a is known and m is to be determined. It is assumed that $m \in X'$ lies in a lower dimensional Banach space X', allowing for a reduction in the search space.

The problem (5.1.1) is then replaced by

$$\begin{aligned} \underset{m,u^\epsilon}{\text{minimize}} \quad & \mathcal{J}(a^\epsilon, u^\epsilon) \\ \text{subject to} \quad & c(a^\epsilon, u^\epsilon) = 0, \\ & a^\epsilon(x) = a(x/\epsilon, m(x)). \end{aligned} \tag{5.1.3}$$

The following is a summary of the different numerical approaches for microscale inversion.

I. **Full inverse problem** (Microscale inversion of the full model).

   The full inverse problem (5.1.1) is ill-posed and computationally expensive. Therefore, we omit this case from our computations.

II. a. **Analytic solver** (Microscale inversion of the effective model).

   If the closed form of the effective coefficient $A(x, m(x))$ corresponding to the parametrized coefficient $a^\epsilon(x) = a(x/\epsilon, m(x))$ is known, the effective inverse problem can also be formulated in terms of microstructure. Here, macroscopic solvers for the effective equation are used to make predictions of the forward model in the optimization problem

$$\underset{m,U}{\text{minimize}}\ \mathcal{J}^0(A, U) \quad \text{subject to} \quad c^0(A, U) = 0, \quad A = A(\cdot, m). \tag{5.1.4}$$

   b. **HMM** (Microscale inversion of the effective model).

Often, the explicit form of the homogenized coefficient corresponding to a^ϵ is not known, and therefore the term $A(\cdot, m)$ in (5.1.4) cannot be directly computed. This issue can be overcome numerically with the heterogeneous multiscale method, or HMM, introduced by E and Engquist [32]. HMM provides a framework for the design of methods that capture macroscale properties of a system using microscale information. The HMM formulation of the minimization problem is

$$\begin{aligned} &\underset{m,U}{\text{minimize}} \quad \mathcal{J}^0(A_{HMM}, U_{HMM}) \\ &\text{subject to} \quad c^{HMM}(a^\epsilon, U_{HMM}) = 0, \quad a^\epsilon(x) = a(x/\epsilon, m(x)). \end{aligned} \tag{5.1.5}$$

Here, the constraint $c^{HMM}(a^\epsilon, U_{HMM}) = 0$ is satisfied when U_{HMM} is the HMM solution corresponding to (5.0.1). The use of HMM allows for the ability to evaluate the functional $\mathcal{J}^0(A_{HMM}, U_{HMM})$ without explicit knowledge of A_{HMM}.

III. **Two-stage solver** (Effective inversion coupled with microscale recovery). Another option is to first solve the minimization problem (5.1.2) and then determine the microscale parameter from the recovered effective coefficient. This idea is formulated as the two-stage procedure,

$$\begin{cases} (\hat{A}, \hat{U}) = \ \text{argmin} \quad \mathcal{J}^0(A, U) \text{ subject to } c^0(A, U) = 0, \\ \qquad\qquad \underset{m}{\text{minimize}} \quad \|A(\cdot, m) - \hat{A}\|^2. \end{cases} \tag{5.1.6}$$

Remark 5.1.1. The main objective of this work is to probe the effects of a microscale parametrization on the reconstructed coefficients. The choice of a regularization functional $\mathcal{R}$ and the constant $\alpha \geq 0$ in (5.1.1) and (5.1.2) is a research

topic on its own, and in this work we concentrate on issues concerning the data fidelity term by setting $\alpha = 0$.

5.2 Multiscale analysis for the inverse conductivity problem

In this section we provide analysis for the inverse coefficient problem corresponding to (5.0.1) with $b^\epsilon = 0$. Let Ω be an open, bounded region in $\mathbb{R}^d$, $d \geq 2$, that has a sufficiently smooth boundary $\partial\Omega$. In applications, Ω is thought of as a conducting medium with spatially varying electrical properties. The steady state voltage potential u solves the equation

$$-\text{div}(\gamma \nabla u) = 0 \text{ in } \Omega. \tag{5.2.1}$$

The coefficient γ, referred to as the conductivity, is in general a uniformly positive definite, symmetric, $d \times d$ matrix; if γ is scalar we say that the conductivity is isotropic, in all other cases it is called anisotropic [84]. In the next sections we will model multiscale and effective conductivities by $\gamma(x) = a^\epsilon(x)$ and $\gamma(x) = A(x)$ respectively.

The aim of inverse conductivity problems is to determine γ using multiple boundary measurements.

Definition 5.2.1. For $f, g \in H^{1/2}(\partial\Omega)$ let $u \in H^1(\Omega)$ be the weak solution to (5.2.1) subject to $u|_{\partial\Omega} = f$, and let v be an arbitrary function in $H^1(\Omega)$ that satisfies $v|_{\partial\Omega} = g$.

The Dirichlet-to-Neumann map $\Lambda_\gamma : H^{1/2}(\partial\Omega) \to H^{-1/2}(\partial\Omega)$ is defined

by

$$\langle \Lambda_\gamma f, g \rangle = \int_\Omega \gamma(x) \nabla u(x) \cdot \nabla v(x) dx. \tag{5.2.2}$$

We will summarize the proof in [84] that the Dirichlet-to-Neumann map is well defined and bounded. Suppose v_1, v_2 are functions in $H^1(\Omega)$ satisfying $v_1|_{\partial\Omega} = v_2|_{\partial\Omega} = g$. Then,

$$\int_\Omega -\mathrm{div}(\gamma \nabla u)(v_1 - v_2) dx = \int_\Omega \gamma \nabla u \cdot \nabla (v_1 - v_2) dx = 0,$$

and therefore the right hand side of (5.2.2) is independent of the choice of the function v satisfying $v|_{\partial\Omega} = g$. For fixed u, the right hand side of (5.2.2) defines a bounded linear operator on $H^{1/2}(\partial\Omega)$ since there exists a $v \in H^1(\Omega)$ with $v|_{\partial\Omega} = g$ and $|v|_{H^1(\Omega)} \leq C|g|_{H^{1/2}(\partial\Omega)}$. This ensures existence and uniqueness of the Dirichlet-to-Neumann map. The inequalities below prove that the Dirichlet-to-Neumann map is a bounded map from $H^{1/2}(\partial\Omega) \to H^{-1/2}(\partial\Omega)$:

$$\begin{aligned} \int_\Omega \gamma \nabla u \cdot \nabla v dx &\leq C \|u\|_{H^1(\Omega)} \|v\|_{H^1(\Omega)} \\ &\leq C \|f\|_{H^{1/2}(\partial\Omega)} \|g\|_{H^{1/2}(\partial\Omega)}. \end{aligned}$$

The inverse boundary value problem of Calderón [19], also known as the inverse conductivity problem or electrical impedance tomography, is to recover γ from knowledge of the Dirichlet-to-Neumann map Λ_γ. For recent results involving uniqueness and reconstruction, see [17, 22, 85]. In order to resolve stability issues [2] some approaches replace a-priori regularity assumptions for γ with different assumptions that are more suited for applications. These ideas

are related to the current task of extracting microscale properties from effective boundary measurements.

Conductivities with special anisotropy

Now we consider inverse conductivity problems for anisotropic conductivities, $\gamma(x) = A$, where A is a matrix function taking values in $\mathbb{R}^{2\times 2}$. We will also include the prior knowledge of a parametrization $A = A(x, m(x))$ for a scalar function $m(x) \in L^\infty(\Omega)$ and symmetric matrix A. Then, $m \to A(\cdot, m)$ is a matrix-valued function with derivative $D_m A$. Uniqueness and stability results for the inverse conductivity problem are given in [3] for cases where the coefficient satisfies admissibility conditions (Definition 2.2 in [3]).

Definition 5.2.2. For a measureable set $D \subset \mathbb{R}^d$, we say $A \in \mathcal{M}(\lambda^{-1}, \lambda, D)$ if $A \in H^{1,p}(D)$, and

$$\lambda^{-1}|\xi|^2 \leq A(z)\xi \cdot \xi \leq \lambda|\xi|^2,$$

for any $\xi \in \mathbb{R}^d$ and a.e. $z \in D$.

Definition 5.2.3. We say $A(\cdot,\cdot) \in \mathcal{H}$ if the following conditions are satisfied:

$$\begin{aligned} A &\in H^{1,p}(\Omega, [\lambda^{-1}, \lambda], \mathrm{Sym}_n), \\ D_m A &\in H^{1,p}(\Omega, [\lambda^{-1}, \lambda], \mathrm{Sym}_n), \\ \mathrm{supess}_{m\in[\lambda^{-1},\lambda]} &\big(\|A(\cdot, m)\|_{L^p(\Omega)} + \|D_x A(\cdot, m)\|_{L^p(\Omega)}, \\ &\quad + \|D_m A(\cdot, m)\|_{L^p(\Omega)} + \|D_m D_x A(\cdot, m)\|_{L^p(\Omega)} \big) \leq E, \end{aligned}$$

$\lambda^{-1}|\xi|^2 \leq A(x, m)\xi \cdot \xi \leq \lambda|\xi|^2$ for a.e. $x \in \Omega$ and all $m \in [\lambda^{-1}, \lambda], \xi \in \mathbb{R}^d$.

In addition, the following monotonicity condition must also be satisfied:

$$D_m A(x,m)\xi \cdot \xi \geq E^{-1}|\xi|^2 \text{ for a.e. } x \in \Omega \text{ and all } m \in [\lambda^{-1}, \lambda], \xi \in \mathbb{R}^d. \quad (5.2.3)$$

The following theorem, adapted to our context, is from [3]. It gives a global uniqueness result for matrices $A(\cdot,\cdot) \in \mathcal{H}$.

Theorem 5.2.1 (Adapted from Theorem 2.1 in Alessandrini, Gaburro, 2001). *Given $p > d$, let Ω be a bounded Lipschitz domain with constants L, r, h. Let m_1, m_2 satisfy*

$$\lambda^{-1} \leq m_1(x), m_2(x) \leq \lambda \text{ for all } x \in \Omega, \quad (5.2.4)$$

$$\|m_1\|_{H^{1,p}(\Omega)}, \|m_2\|_{H^{1,p}(\Omega)} \leq E, \quad (5.2.5)$$

Let A be sufficiently bounded and monotone; then,

$$\|A(x,m_1(x)) - A(x,m_2(x))\|_{L^\infty(\partial\Omega)} \leq C\|\Lambda_{A(x,m_1(x))} - \Lambda_{A(x,m_2(x))}\|_*.$$

Here C is a constant that depends only on $d, p, L, r, diam(\Omega), \lambda$ and E.

Theorem 5.2.2 (Adapted from Theorem 2.4 in Alessandrini, Gaburro, 2001). *Suppose m_1, m_2 satisfy (5.2.4) and (5.2.5). Suppose also that Ω can be partitioned into a finite number of domains $\{\Omega_j\}_{j \leq N}$, with $m_1 - m_2$ analytic on each $\overline{\Omega}_j$. Then, $\Lambda_{A(\cdot,m_1)} = \Lambda_{A(\cdot,m_2)}$ implies that $A(\cdot,m_1) = A(\cdot,m_2)$ in Ω.*

This theorem will be used to determine whether microscale features depend continuously on data from the homogenized model. The next section will describe the related problem of inverse homogenization.

Inverse homogenization

We consider inverse homogenization of the Dirichlet problem

$$-\text{div}\,(a^\epsilon \nabla u^\epsilon) = f \text{ in } \Omega, \qquad u^\epsilon = 0 \text{ on } \partial\Omega. \tag{5.2.6}$$

The goal of inverse homogenization is to recover the coefficient a^ϵ from macroscale data d_* of the form $d_* = \mathcal{G}(U, \nabla U, x)$, where U is the solution to an effective problem of the form

$$-\text{div}\,(A\nabla U) = f \text{ in } \Omega, \qquad U = 0 \text{ on } \partial\Omega. \tag{5.2.7}$$

In [28], the problem is re-cast using the geometric framework underlying homogenization. Here, we will parametrize the conductivity itself in order to re-formulate the problem as an optimization problem involving a low dimensional search space.

Microscale Parametrization

Explicit solutions of the homogenized equation (5.2.6) can be found for problems in the case $d = 1$, and also in certain higher dimensional models that have a one-dimensional character, such as those describing layered media [51]. We will use the following examples of models that include a microscale parametrization, depicted in Figure 5.1.

Let $m \in L^\infty(\Omega)$ be a function taking values in an interval $I = [\lambda^{-1}, \lambda]$. We consider functions $a(y, \eta)$ that are $Y-$ periodic in y, $Y = [0, \lambda]^2$. Then, the

multiscale conductivity a^ϵ is characterized by

$$a^\epsilon(x) = a(x/\epsilon, m(x)). \tag{5.2.8}$$

A. **Volume fraction.** An example of a function that characterizes a two-phase medium that takes values from the functions $a_1(y) = a_1(y_2)$ and $a_2(y) = a_2(y_2)$ with the respective volume fractions $\frac{\eta}{|Y|}$ and $\frac{1-\eta}{|Y|}$ respectively.

$$a(y,\eta) = \begin{cases} a_1(y_2) & 0 \le y_1 < \eta \\ a_2(y_2) & \eta \le y_1 < \lambda \end{cases}. \tag{5.2.9}$$

B. **Amplitude.** Here we include a damping term η that restricts the oscillations of a multiscale function. For $a_0 > 0$ and a $\lambda-$periodic function $a_1 \in L^\infty(\mathbb{R})$,

$$a(y,\eta) = a_0 + \eta a_1(y_2). \tag{5.2.10}$$

C. **Angle.** The assumption (5.2.8) is modified in the third case. Here, the conductivity a^ϵ is characterized by a $Y-$periodic function $\hat{a} \in L^\infty(\mathbb{R}^2)$, and a spatially varying rotation matrix $\sigma_{m(x)}$,

$$a^\epsilon(x) = \hat{a}(\sigma_{m(x)}x/\epsilon), \qquad \sigma_\eta = \begin{pmatrix} \cos\eta & \sin\eta \\ -\sin\eta & \cos\eta \end{pmatrix}. \tag{5.2.11}$$

In the following we will restrict our attention to functions a satisfying $\lambda^{-1} \le a(y,\eta) \le \lambda$ for all η in I and $y \in \Omega$, and choose a_0, a_1 and a_2 accordingly.

Effective coefficients

In this section we derive the closed form of the homogenized coefficient matrix corresponding to parametrized functions a^ϵ defined in the previous section. For the model problems we consider, the spatial dependence of effective

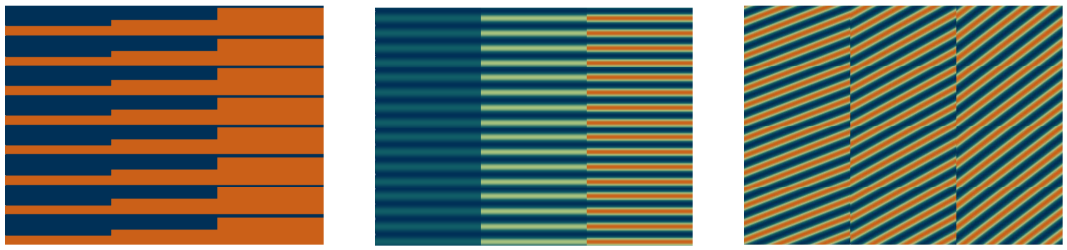

Figure 5.1: **Periodic microstructure model for layered materials.** Oscillatory conductivities with spatially varying microscale components. From left to right: volume fraction, amplitude, and angle.

coefficient is determined only by m, that is, $A(x, m(x)) = A(m(x))$. The following lemma describes the effective coefficient corresponding to almost periodic functions. The averaging operator is denoted $\langle f \rangle_X = \frac{1}{|X|} \int_X f(y)dy$, where $|X|$ is the volume of the set $X \subset \mathbb{R}^2$.

Lemma 5.2.1. *Suppose $a^\epsilon(x) = \tilde{a}(x/\epsilon, m(x))$, where the function $\tilde{a}(y, \eta) \in \mathcal{M}(\lambda^{-1}, \lambda; Y \times I)$ is isotropic, smooth in x and Y—periodic in y. If in addition the equation $\tilde{a}(y, \eta) = \tilde{a}(y_2, \eta)$ holds for all $\eta \in I, y \in Y$, then the homogenized coefficient corresponding to a^ϵ is a symmetric matrix $A(x, m) = A(m) \in \mathcal{M}(\lambda^{-1}, \lambda; I)$ that has the form*

$$A(m) = diag(\langle \tilde{a}(\cdot, m) \rangle_Y, \langle \tilde{a}(\cdot, m)^{-1} \rangle_Y^{-1}). \tag{5.2.12}$$

Proof. Homogenization theory for locally periodic functions [51, 69] provides the explicit form of A, the homogenized coefficient corresponding to a^ϵ. For $m \in I$,

$$A(m) = \frac{1}{|Y|} \int_Y (\tilde{a}(y, m)Id + \tilde{a}(y, m)\nabla_y \chi)dy, \tag{5.2.13}$$

where $\chi = (\chi_1, \chi_2)$ solves the cell problems:

$$-\nabla_y \cdot (\tilde{a}(y,m)\nabla_y \chi) = \nabla_y \cdot \tilde{a}(y,m) Id \tag{5.2.14}$$

with the constraint $\chi(y,m)$ is $Y-$periodic in y and $\int_Y \chi(y,m)dy = 0$. Since we further assumed that $\tilde{a}$ is a function only of x and y_2, $\tilde{a} = \tilde{a}(y_2,m)$, the solutions to the cell problem (5.2.14) are of the form $\chi = (\chi_1(y_2,m), \chi_2(y_2,m))$. Therefore, (5.2.14) is equivalent to

$$-\frac{\partial}{\partial y_2}(\tilde{a}(y_2,m)\frac{\partial}{\partial y_2}\chi_1) = 0,$$
$$-\frac{\partial}{\partial y_2}(\tilde{a}(y_2,m)\frac{\partial}{\partial y_2}\chi_2) = \frac{\partial}{\partial y_2}\tilde{a}(y_2,m).$$

Integration from 0 to y_2 gives

$$\tilde{a}(y_2,m)\frac{\partial \chi_1}{\partial y_2} = c_1, \tag{5.2.15}$$

$$\tilde{a}(y_2,m)\frac{\partial \chi_2}{\partial y_2} = -\tilde{a}(y_2,m) + d_1, \tag{5.2.16}$$

for some constant functions $c_1(m), d_1(m)$. Since $\tilde{a}$ is strictly positive, we can divide (5.2.15) and (5.2.16) by $\tilde{a}(y_2,m)$ and integrate from 0 to y_2 again

$$\chi_1 = c_1 \int_0^{y_2} \frac{1}{\tilde{a}(\xi,m)} d\xi + c_2, \qquad \chi_2 = -y_2 + d_1 \int_0^{y_2} \frac{1}{\tilde{a}(\xi,m)} d\xi + d_2.$$

Now, using periodicity, $\chi_l(0,m) = \chi_l(\lambda,m)$ it follows that that $c_1 = 0$, and $d_1 = \langle \tilde{a}(\cdot,m)^{-1} \rangle_Y^{-1}$. Therefore (5.2.15) and (5.2.16) become

$$\tilde{a}(y_2,m)\frac{\partial \chi_1}{\partial y_2} = 0,$$
$$\tilde{a}(y_2,m)\frac{\partial \chi_2}{\partial y_2} = -\tilde{a}(y_2,m) + \langle \tilde{a}(\cdot,m)^{-1} \rangle_Y^{-1}.$$

Substituting these expressions into (5.2.13) results in the closed form for the effective coefficient (5.2.12). As a result, A is a symmetric matrix function and for $\xi \in \mathbb{R}^2$ and $m \in I$,

$$\lambda^{-1}|\xi|^2 \leq \langle \tilde{a}(\cdot, m)^{-1} \rangle_Y^{-1} |\xi|^2 \leq (A(m)\xi, \xi),$$
$$|A(m)\xi| \leq |\langle \tilde{a}(\cdot, m) \rangle_Y \xi| \leq \lambda |\xi|.$$

□

Now we can derive the homogenized coefficients corresponding to a^ϵ of the form (5.2.9) and (5.2.10) and prove the main result using Theorem 5.2.2.

Theorem 5.2.2. *Suppose m_1, m_2 satisfy (5.2.4) and (5.2.5). Suppose also that $m_1 - m_2$ is piecewise analytic on Ω. Let $a_i^\epsilon(x) = a(x/\epsilon, m_i(x))$ be a multiscale coefficient of the form (5.2.9) or (5.2.10), and denote the corresponding homogenized coefficient by $A(m_i)$, $i = 1, 2$. Then, $\Lambda_{A(m_1)} = \Lambda_{A(m_2)}$ implies that $m_1 = m_2$ in Ω and there is a constant $C > 0$ with*

$$\|a^\epsilon(m_1) - a^\epsilon(m_2)\| \leq C \|\Lambda_{A(m_1)} - \Lambda_{A(m_2)}\|.$$

Proof. We can check the smoothness and monotonicity assumptions by directly calculating the homogenized coefficients. Applying Lemma 5.2.1 results in

$$A(m) = diag(\langle \tilde{a}(\cdot, m) \rangle_Y, \langle \tilde{a}(\cdot, m)^{-1} \rangle_Y^{-1})$$

Therefore, the boundedness of $\tilde{a}$ implies the boundedness of A, and $D_m A(m)$ is monotone in the sense of (5.2.3) if there is a constant $E > 0$ with

$$D_m \langle \tilde{a}(\cdot, m)^{-1} \rangle_Y^{-1} > E \text{ and } D_m \langle \tilde{a}(\cdot, m) \rangle_Y > E.$$

In other words, we require that the monotonicity of the function $\tilde{a}$ is preserved after averaging and taking the harmonic mean. Monotonicity can be directly verified in both cases (5.2.9) and (5.2.10). Therefore, the assumptions of Theorem 5.2.2 and 5.2.1 are satisfied and $m_1 = m_2$ for a.e. x in Ω, along with the stability result.

□

We also will describe the effective coefficient corresponding to an angular parametrization.

Lemma 5.2.3. *Suppose a^ϵ is of the form (5.2.11) with $\hat{a}(y) = \hat{a}(y_2)$ for all $y = (y_1, y_2)$. Also, suppose that m is a constant function, again denoted m. The corresponding homogenized coefficient has the form*

$$A(m) = \langle \hat{a} \rangle_Y Id + \left(\langle \hat{a}^{-1} \rangle_Y^{-1} - \langle \hat{a} \rangle_Y \right) \begin{pmatrix} \cos^2 m & \cos m \sin m \\ \cos m \sin m & \sin^2 m \end{pmatrix}. \quad (5.2.17)$$

Proof. Let $\sigma = \sigma_m$. The homogenized coefficient corresponding to $\hat{a}$ is a known matrix $\hat{A} = diag(\langle \hat{a} \rangle_Y, \langle \hat{a}^{-1} \rangle_Y^{-1})$. For a bounded set $X \subset \mathbb{R}^2$, consider the scalar problems

$$\int_X \nabla \psi \cdot \hat{a}(x/\epsilon) \nabla u^\epsilon dx = 0, \quad \forall \psi \in H_0^1(X) \quad \text{for } u^\epsilon \in H_0^1(X),$$
$$\int_X \nabla \psi \cdot \hat{A} \nabla U dx = 0, \quad \forall \psi \in H_0^1(X) \quad \text{for } U \in H_0^1(X).$$

Now consider the change of variables $x = \sigma y$ where σ is an orthogonal

transformation from $\mathbb{R}^2$ to $\mathbb{R}^2$. We obtain the Dirichlet problems for $X' = \sigma^{-1}X$

$$\int_{X'} \nabla_y \psi \cdot \hat{a}(\sigma y/\epsilon) \nabla_y u^\epsilon(\sigma y) dy = 0,$$
$$\int_{X'} \nabla_y \psi \cdot \sigma \hat{A} \sigma^{-1} \nabla_y U(\sigma y) dy = 0.$$

Since $u^\epsilon(\sigma y) \rightharpoonup U(\sigma y)$ in $H_0^1(X')$, it follows that the homogenized coefficient for $a^\epsilon(x)$ is $\sigma \hat{A} \sigma^{-1}$. □

Remark 5.2.1. In this case, the derivative matrix function

$$D_m A = \left(\langle \hat{a}^{-1} \rangle_Y^{-1} - \langle \hat{a} \rangle_Y \right) \begin{pmatrix} -\sin 2m & \cos 2m \\ \cos 2m & \sin 2m \end{pmatrix}$$

has eigenvalues ± 1. Therefore, the monotonicity assumption of Theorem 5.2.2 cannot be directly applied. However, our numerical results (see §5.3 and §5.4) indicate that a microscale parametrization of the angle is also determined from the effective Dirichlet-to-Neumann map.

Homogenization of periodic cell structures

In two dimensions, the homogenized form of a^ϵ is generally not known explicitly. We will consider two examples that can be used to model periodic cell structures. A typical cell is modeled by the set $Y = [0, \lambda]^2$, $\lambda > 1$. For $\eta' \in I = [\lambda^{-1}, \lambda]$, we denote the interior of a cell by the set $Y' = \{(y_1, y_2) \in Y \mid y_1 < \eta', y_2 < \eta'\}$ and let a_1, a_2 be positive constants.

D. **Cell wall thickness.** In the first example we again consider a spatially vary-

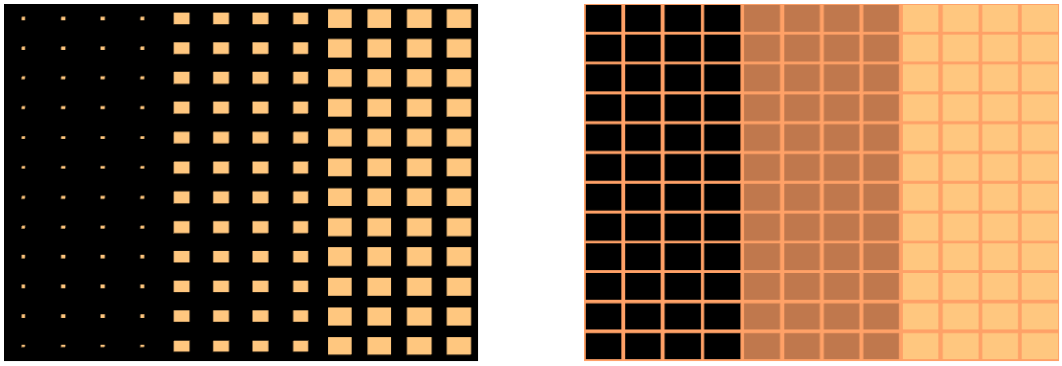

Figure 5.2: **Microscale model for periodic cell structures.** Piecewise constant functions are used to model cell structures that have spatially varying membrane thickness (left) and interior properties (right).

ing parameter that determines the thickness of the cell walls,

$$a^\epsilon(x) = a(x/\epsilon, m(x)), \qquad a(y,\eta) = \begin{cases} a_1 & y \in \frac{\eta}{|Y|}Y \\ a_2 & \text{otherwise} \end{cases}. \tag{5.2.18}$$

E. **Interior diffusivity.** In the second consider a configuration of cells with a fixed geometry that possess spatially varying diffusivity on the interior of the cell,

$$a^\epsilon(x) = a(x/\epsilon, m(x)), \qquad a(y,\eta) = \begin{cases} \eta a_1 & y \in Y' \\ a_2 & \text{otherwise} \end{cases}. \tag{5.2.19}$$

Lemma 5.2.4. *Suppose a^ϵ is of the form (5.2.18) or (5.2.19). Then, the homogenized coefficient corresponding to a^ϵ is an isotropic matrix function A defined by*

$$A(m) = \bar{a}(m) Id, \tag{5.2.20}$$

$$\bar{a}(m) = \frac{1}{|Y|}\int_0^\lambda \left(\int_0^\lambda \frac{1}{a(y,m)} dy_1 \right)^{-1} dy_2. \tag{5.2.21}$$

Proof. Homogenization theory for locally periodic functions [51, 69] provides the explicit form of $A(\eta)$, the homogenized coefficient corresponding to $a(y,\eta)$. For $\eta \in I$,

$$A(\eta) = \frac{1}{|Y|}\int_Y (a(y,\eta)Id + a(y,\eta)\nabla_y \chi)dy, \tag{5.2.22}$$

where $\chi = (\chi_1, \chi_2)$ solves the cell problems

$$-\nabla_y \cdot (a(y,\eta)\nabla_y \chi) = \nabla_y \cdot a(y,\eta)Id, \tag{5.2.23}$$

with the constraint $\chi_i(y,\eta)$ is $Y-$periodic in the second variable and

$$\int_Y \chi_i(y,\eta)dy = 0.$$

The solutions to the cell problems (5.2.23) are equivalent to

$$\begin{aligned} &\frac{\partial}{\partial y_i}\left(a(y,\eta)\frac{\partial \chi_k}{\partial y_i}\right) = -\frac{\partial}{\partial y_i}a(y,\eta), && i = 1,2, \quad k = i, \\ &\frac{\partial}{\partial y_i}\left(a(y,\eta)\frac{\partial \chi_k}{\partial y_i}\right) = 0, && i = 1,2, \quad k \neq i. \end{aligned} \tag{5.2.24}$$

Furthermore, the function $a(y,\eta)$ satisfies the condition of cubic symmetry (see [51]), and therefore the effective coefficient is isotropic; that is, (5.2.20) holds for a function $\bar{a}$ to be determined. As a consequence, $\bar{a}$ can be calculated using only the solution to (5.2.24) for $i = k = 1$. Integration from 0 to y_1 gives

$$a(y,\eta)\frac{\partial \chi_1}{\partial y_1} = -a(y,\eta) + c_1, \tag{5.2.25}$$

where c_1 is a function of only η and y_2. Since a is positive, we can divide by a and integrate from 0 to y_1 again, giving

$$\chi_1 = -y_1 + c_1\int_0^{y_1} \frac{1}{a(y,\eta)}dy_1 + c_2,$$

where c_2 is also a function of only η and y_2. Applying the periodic boundary conditions $\chi_1|_{y_1=0} = \chi_1|_{y_1=1}$ results in the determination of c_1 as

$$c_1(y_2, \eta) = \left(\int_0^\lambda \frac{1}{a(y, \eta)} dy_1 \right)^{-1}.$$

Therefore (5.2.25) becomes

$$a(y, \eta) \frac{\partial}{\partial y_1} \chi_1 = -a(y, \eta) + \left(\int_0^\lambda \frac{1}{a(y, \eta)} dy_1 \right)^{-1}.$$

Substituting these expressions into (5.2.22) results in the closed form for the effective coefficient (5.2.21). □

We can now show that the homogenized cell structures are monotone in the sense of (5.2.3) and prove the next result.

Theorem 5.2.5. *Theorem 5.2.2 also holds for $a^\epsilon(x) = a(x/\epsilon, m(x))$ of the form (5.2.18) or (5.2.19) with a_1, a_2 chosen such that $\left\langle \frac{\partial a}{\partial m}(\cdot, m) \right\rangle_Y > \lambda^{-4} E > 0$ for all $m \in I$.*

Proof. Applying Lemma 5.2.4 results in $A(m) = \bar{a}(m) Id$, for $\bar{a}$ in (5.2.21). The boundedness of $\bar{a}$ is a direct consequence of the boundedness of a. Defining the

function $\varphi \in L^\infty([0,\lambda]\times I)$ by $\varphi(y_2,m) = \lambda^{-1}\int_0^\lambda \frac{1}{a(y,m)}dy_1$, it follows that

$$\begin{aligned} D_m\bar{a}(m) &= \lambda^{-1}\int_0^\lambda \frac{\partial}{\partial m}\left[(\varphi(y_2,m))^{-1}\right]dy_2 \\ &= -\lambda^{-1}\int_0^\lambda \left[(\varphi(y_2,m))^{-2}\right]\frac{\partial \varphi}{\partial m}(y,m)dy_2 \\ &= \lambda^{-2}\int_0^\lambda\int_0^\lambda \frac{\frac{\partial a}{\partial m}(y,m)}{(\varphi(y_2,m)a(y,m))^2}dy_1dy_2 \\ &\geq \lambda^{-4}\left\langle \frac{\partial a}{\partial m}(\cdot,m)\right\rangle_Y. \end{aligned}$$

Therefore, the requirement that $\left\langle \frac{\partial a}{\partial m}(\cdot,m)\right\rangle_Y > \lambda^{-4}E$ ensures that the monotonicity condition $D_m\bar{a}(y,m) > E > 0$ is satisfied for every $m \in I$ and $y \in \Omega$.

□

Remark 5.2.2. So far, we have only considered the parametrization of one microscale parameter (e.g., angle or amplitude). Our numerical results in §5.3 also include the parametrization of multiple features using the map

$$(m,n) \to A(m,n).$$

In cases where the effective coefficient is not known, a numerical approximation of the effective problem can be estimated with multiscale methods such as HMM, described in Chapter 3. Our numerical results indicate that microscale details can be gleaned from macroscopic boundary measurements.

5.3 Computational methods for inversion

For the optimization problems (5.1.4) and (5.1.5), predictions of the effective model are simulated using an analytic forward solver and FEM-HMM (see IIa and IIb in Section 5.1). The inversion results also include errors produced using a two-stage solver (III in Section 5.1) for the minimization problem (5.1.6). The forward problems (5.0.1) and (5.0.2) are solved for $f = 0$, and imposed Dirichlet boundary conditions $g^{(1)}, \dots g^{(K)}$.

Forward solvers

Let $\mathcal{T}_h$ be a regular triangulation of Ω with microscopic resolution $h < \epsilon$, and let X_h be the corresponding piecewise linear finite element space. The finite element solution $u_h^{(k)} \in g^{(k)} + X_h$ to the full problem (5.2.6) has the variational formulation

$$\int_\Omega \nabla v(x) \cdot a^\epsilon(x) \nabla u_h^{(k)}(x) dx + \int_\Omega b^\epsilon(x) u_h^{(k)}(x) dx = 0, \tag{5.3.1}$$

for all $v \in X_h$. Let $\mathcal{T}_H$ be a regular triangulation of Ω with macroscopic resolution $H > \epsilon$, and let X_H be the corresponding piecewise linear finite element space. The macroscopic finite element solution $U^{(k)} \in g^{(k)} + X_H$ to the effective problem (5.2.7) satisfies

$$\int_\Omega \nabla V(x) \cdot A(x) \nabla U^{(k)}(x) dx + \int_\Omega \overline{b}(x) U^{(k)}(x) dx = 0, \tag{5.3.2}$$

for all $V \in X_H$. From the previous section, we have that for all $V \in X_H$, the FE-HMM solution $U^{(k)}_{HMM} \in g^{(k)} + X_H$ satisfies

$$\int_\Omega \nabla V(x) \cdot A_{HMM}(x) \nabla U^{(k)}_{HMM}(x) dx + \int_\Omega \overline{b}(x) U^{(k)}_{HMM}(x) dx = 0, \qquad (5.3.3)$$

where A_{HMM} is estimated by microscale solvers on local subdomains.

Discrete inverse problem

We will now describe the computation of the discrete observations and predictions. The function $\mathcal{G} = \mathcal{G}(u, \nabla u, x)$ will be common to both the observation and prediction operators. We denote by $\mathcal{G}^h$ the restriction of $\mathcal{G}$ to discrete solutions that are resolved on an $O(h)$ microscopic mesh, and similarly we denote by $\mathcal{G}^H(U, \nabla U, x)$ the restriction of $\mathcal{G}$ to discrete solutions that are resolved on a macroscopic mesh of $O(H)$.

I. The synthetic data is created in two steps. First, the full solution discretized on a microscopic mesh $\mathcal{T}_h$ is used to compute $\mathcal{G}^h(u^\epsilon, \nabla u^\epsilon, x)$. Then, the observed data is set to be

$$\mathscr{G}(m) = d_* = \Pi^H \mathcal{G}^h(u^\epsilon, \nabla u^\epsilon, x); \qquad c(a^\epsilon(\cdot, m), u^\epsilon) = 0,$$

where Π^H is a projection operator from $\mathcal{T}_h$ onto $\mathcal{T}_H$.

II. Predictions take the form

$$\mathscr{F}(\hat{m}) = \mathcal{G}^H(U, \nabla U, x); \quad c^0(A(\hat{m}), U) = 0$$

where the solutions are computed using a forward solver on the macroscale mesh $\mathcal{T}_H$. In the case where $A(\hat{m})$ is unknown, the state equation $c^0(A,U)=0$ is replaced by the state equation $c^{HMM}(a^\epsilon(\cdot,\hat{m}),U_{HMM})=0$ corresponding to the HMM solution (5.3.3). In the case of the inverse conductivity problems, observed data and predictions are set to be the discrete Dirichlet-to-Neumann maps determined by the Dirichlet conditions and solutions of the forward model.

a. The discrete problem corresponding to the effective inverse problem (5.1.4) is

$$\begin{aligned} \underset{m,U}{\text{minimize}} \quad & \|\mathcal{G}^H(U,\nabla U,x)-d_*\| \\ \text{subject to} \quad & c^0(A,U)=0, \\ & A=A(\cdot,m), \end{aligned} \tag{5.3.4}$$

where C^0 is satisfied when U solves (5.3.2).

b. The HMM-reduced model (5.1.5) becomes

$$\begin{aligned} \underset{m,U_{HMM}}{\text{minimize}} \quad & \|\mathcal{G}^H(U_{HMM},\nabla U_{HMM},x)-d_*\| \\ \text{subject to} \quad & c^{HMM}(a^\epsilon,U_{HMM})=0, \\ & a^\epsilon=a(\cdot/\epsilon,m), \end{aligned} \tag{5.3.5}$$

where c^{HMM} is satisfied when U_{HMM} solves (5.3.3).

III. Finally, the two-stage procedure (5.1.6) is discretized as

$$\begin{cases} (\hat{A},\hat{U})= \text{ argmin} & \|\mathcal{G}^H(U,\nabla U,x)-d_*\| \\ \text{subject to} & c^0(A,U)=0, \\ \underset{m}{\text{minimize}} & \|A(\cdot,m)-\hat{A}\|. \end{cases} \tag{5.3.6}$$

Remark 5.3.1. We emphasize that the synthetic data is simulated by first solving the full problem (5.3.1) on a fine mesh $\mathcal{T}_h$. The fully resolved solution is then projected onto a coarse grid $\mathcal{T}_H$ using a smoothing operator, e.g., windowed averaging or interpolation. This provides a framework for microscale inversion that avoids the major pitfalls of committing an "inverse crime."

5.4 Numerical Results

In §5.2, the parameter m is chosen to be a scalar function that satisfies the requirements of Theorem 5.2.2. In our numerical experiments, the unknown microscale parameter m is a vector with N components, $m \in (0,1)^N$. This vector is used to determine the coefficients of a piecewise constant function defined on a partition of the domain $\{\Omega_k\} \subset \Omega$, $1 \leq k \leq N$, $\cup_k \Omega_k = \Omega$.

The inversion errors are calculated using the least squared distance between the true parameter m^* and a predicted parameter $\hat{m}$. Since $0 < m < 1$, we choose to use the absolute error.

Inverse conductivity ($b^\epsilon = 0$)

The problems (5.0.1), (5.0.2) are discretized on the domain $\Omega = [0,2] \times [0,2]$. We set $f = 0$ and prescribe the Dirichlet boundary conditions, $G = \{g_1, \dots g_K\}$. The coefficient a^ϵ is defined for a given vector $m^* \in (0,1)^N$ by (**??**) using the partition $\Omega_k = [\frac{2(k-1)}{N}, \frac{2k}{N}) \times [0,2)$, $1 \leq k \leq N$.

In the following numerical experiments we use the $K = 4$ boundary con-

ditions $\{x^2, y^2, xy, (xy)^2\}$, and the constants $\epsilon = 1/60$, $H = 1/12$, $h = 1/256$. The microscale cell problems in HMM (equation (3.2.4) in Chapter 3) are solved on the subdomains $I_\delta(x_l) = x_l + 3\epsilon Id$. The projection operator Π^H is set to be convolution with a smoothing kernel. The optimization problems (5.3.4) – (5.3.6) are performed using the MATLAB `lsqnonlin` function. The error is computed as $\|m^* - \hat{m}\|$.

Table 5.1 shows that the analytic and HMM solver perform similarly for all three microstructure models. Inversion using the two-stage solver results in an error that grow linearly with N, the degrees of freedom of the unknown parameter m. This can be attributed to first stage of the two stage solver, where the unknown effective coefficient A has $4N$ degrees of freedom.

Remark 5.4.1. The results in Table 5.2 demonstrate the need for a carefully designed microscale parameters. In certain cases, the solutions to cell problems corresponding to different microscale coefficients a^ϵ are indistinguishable. In particular, for a fixed m, there exists a $\tilde{m}$ such that the homogenized coefficients corresponding to a parametrized volume fraction $m \to a^\epsilon_{VF}(m)$ are equal to the homogenized coefficients corresponding to a parametrized amplitude $\tilde{m} \to a^\epsilon_{AMP}(\tilde{m})$.

These results for the inverse conductivity problem are important to other applications where surface measurements of a medium are used to describe characteristics of the interior. Similar models work in a variety of other areas, including exploration geophysics, mine and rock detection, and reservoir modeling.

Table 5.1: Error in parameter inversion of the multiscale electrical impedance tomography model.

A. Volume Fraction

N	Analytic	HMM	Two-stage
1	0.01654417	0.02539143	0.10816459
2	0.09828509	0.08513511	0.16240264
3	0.10929754	0.10148560	0.27615110
4	0.11633237	0.10527977	0.32224688
5	0.17736705	0.15733702	0.42772383
6	0.42557205	0.18798622	0.38027366

B. Amplitude

N	Analytic	HMM	Two-stage
1	0.03621115	0.04599242	0.04225760
2	0.05374923	0.06188072	0.14315285
3	0.07829441	0.09554321	0.26518266
4	0.06354117	0.06750427	0.24979234
5	0.26919343	0.28371626	1.39133602
6	0.48579157	0.49334067	0.70127957

C. Angle

N	Analytic	HMM	Two-stage
1	0.03577476	0.02663165	0.13256423
2	0.10950838	0.11083198	0.31558807
3	0.19553649	0.16093081	0.72582859
4	0.27517537	0.23496116	0.94267985
5	0.45800627	0.43427778	0.81128416
6	0.66105576	0.41827901	0.38349101

Table 5.2: Error in two-component parameter inversion of the multiscale electrical impedance tomography model.

N	**Angle/ Volume Fraction**	**Angle/ Amplitude**	**Amplitude/ Volume Fraction**
1	0.026535	0.020459	0.185492
2	0.101729	0.075323	0.264703
3	0.267094	0.184916	0.369400

In the next sections we will explore numerical results corresponding to medical imaging and geophysics.

Medical imaging ($b^\epsilon > 0$)

The modeling of wave propagation in heterogeneous media is an important problem in many areas of science and engineering. Current approaches attempt to design methods that account for variations in material microstructures when solving equations of motion in an effective medium [42]. Diffusion in random heterogeneous media is studied in [44, 56].

We will consider a medical imaging technique that uses a combination of optical and ultrasonic waves to determine properties of a medium from surface measurements. In Quantitative Photoacoustic Tomography, (qPAT), optical coefficients are reconstructed from knowledge of the absorbed radiation map [10, 11].

Let $\Omega \subset \mathbb{R}^2$ represent a medium of interest and $\Lambda \subset \mathbb{R}_+$ a set of wavelengths included in the experiment. The density of photons at wavelength λ,

denoted by $u(x,\lambda)$, solves the second-order elliptic equation

$$\begin{cases} -\nabla\cdot(a(x,\lambda)\nabla u(x,\lambda)) + \sigma(x,\lambda)u(x,\lambda) = 0 & x\in\Omega \\ u(x,\lambda) = g(x,\lambda) & x\in\partial\Omega \end{cases}. \tag{5.4.1}$$

Here, a and σ are diffusion and absorption coefficients that are dependent on the wavelength λ. The ultrasound generated by the absorbed radiation is quantified by the Grüneisen coefficient, $\Gamma(x,\lambda)$. The objective of qPAT is to recover (a,σ,Γ) using the measured data from photoacoustic experiments corresponding to an illumination pattern $g(x,\lambda)$.

We will modify the numerical examples from [11] by considering the forward model (5.4.1) with diffusion coefficients that have variations on multiple spatial scales, $a = a^\epsilon$. For simplicity, we will assume that the absorption, diffusion, and Grüneisen coefficients can be expressed as

$$\sigma(x,\lambda) = \sum_{i=1}^{2}\beta_i(\lambda)\sigma_i(x), \qquad a^\epsilon(x,\lambda) = \alpha(\lambda)a^\epsilon(x), \qquad \Gamma(x,\lambda) = \Gamma(x).$$

The measured data takes the form

$$\mathcal{G}(u,\nabla u,x,\Lambda) = \Gamma(x,\lambda)\sigma(x,\lambda)u(x,\lambda), \quad x\in\Omega, \quad \lambda\in\Lambda. \tag{5.4.2}$$

In the numerical experiments, we set $\Omega = (0,2)^2$. The measured data (5.4.2) involves the solutions to (5.4.1) for each wavelength in the set $\Lambda = \{.2,.3,.4\}$. Four illuminations are used for each wavelength. The wavelength dependent components of the coefficients are set to be

$$\beta_1(\lambda) = \frac{\lambda}{\lambda_0}, \quad \beta_2(\lambda) = \frac{\lambda_0}{\lambda}, \quad \alpha(\lambda) = (\lambda/\lambda_0)^{3/2},$$

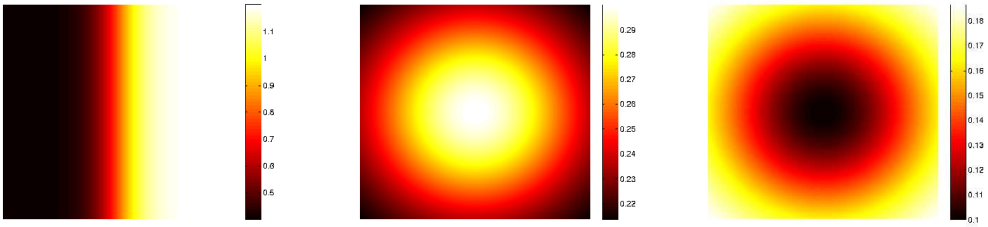

Figure 5.3: **Spatial components of the QPAT model.** Left to right: Grüneisen coefficient $\Gamma(x)$, and absorption component functions $\sigma_1(x)$ and $\sigma_2(x)$.

where the wavelength $\lambda_0 = .3$ normalizes the amplitude of the coefficients. The spatial components of the coefficients are given as

$$\Gamma(x) = .8 + .4\tanh(4x - 4), \qquad a^\epsilon(x) \text{ from (5.2.18) and (5.2.19),}$$

$$\sigma_1(x) = .2 - .1e^{-2\pi|x-x_0|^2}, \qquad \sigma_2(x) = .2 + .1e^{-2\pi|x-x_0|^2}, \qquad x_0 = (1,1).$$

Figure 5.3 contains plots of the spatial components of Γ and σ.

As in [11], the reconstruction errors are given for synthetic data with no noise added. However, errors are introduced from averaging the multiscale solution and projection onto the coarse grid. The parameters used are $\epsilon = 1/60$ $H = 1/12$, $h = 1/256$.

In Table 5.3 we see that parameter inversion using HMM forward solvers is comparable to parameter inversion using an analytic forward solver.

Seismic waveform inversion ($b^\epsilon < 0$)

In exploration geophysics, scientists attempt to determine the geological properties of the Earth's crust that govern the propagation of acoustic waves (see

Table 5.3: Error in parameter inversion of the multiscale quantitative photoacoustic tomography model.

D. Cell Wall Thickness

N	Analytic	HMM	Two-stage
1	0.04466877	0.09868047	0.07346082
2	0.12342225	0.16340499	0.28872537
3	0.29242901	0.29662820	0.30774954
4	0.67723276	0.35198509	0.23976186
5	0.90352620	0.53385607	0.41982687
6	0.87852824	0.62635822	0.39595585

E. Interior Diffusivity

N	Analytic	HMM	Two-stage
1	0.06043366	0.01263081	0.05863142
2	0.10660937	0.03593268	0.10662896
3	0.12042071	0.02412268	0.22820132
4	0.11998803	0.08022306	0.23446521
5	0.29099160	0.26758991	0.16583567
6	0.43617281	0.35820571	0.33752105

[82] for an overview). In full waveform inversion, the goal is to find a subsurface model that produces the best fit to reflection data recorded from seismic surveys. Each prediction is simulated using the physics of the experiment. This corresponds to an inverse problem for partial differential equations where the unknown coefficients represent properties of the sedimentary layers, e.g. velocities, porosity, and saturation.

Full waveform inversion is the result of combining numerical methods for the simulation of wave propagation with optimization techniques to minimize the data misfit term (see [41] for a discussion of multiscale full waveform inversion). Traditional finite element methods (FEM) or finite difference methods (FDM) for wave propagation in the high frequency regime come with a considerably high computational cost due to the highly oscillatory nature of the propagating waves [49].

The forward problem can be modeled in both the time domain and the frequency domain. In theory, both approaches are equivalent, however the choice of model can influence the design of specific numerical methods to optimize performance. An advantage of the frequency domain model is that a coarse discretization of the frequencies can be used to produce images that are free from aliasing [9, 64, 78].

A major hurdle in full waveform inversion is the presence of local minima in the least-squares functional for the data misfit. In [73], adjoint-state methods are used to efficiently calculate the gradient of the least-squares functional and speed up the optimization. We emphasize that in this work we use standard

optimization routines in order to fully study the effects of microscale inversion on the recovered parameter.

We provide numerical examples corresponding to problems that mimic the models used in seismic waveform inversion. Here, the model parameters represent the spatially varying volume fraction, angle, and amplitude of the layers. The forward model is the 2D variable coefficient Helmholtz equation on the square $\Omega = [0,2]^2$, formulated as

$$\nabla \cdot (a(x)\nabla u) + \omega^2 u(x) = \delta(x - x_s) \quad x \in \Omega, \tag{5.4.3}$$

where a is the model parameter that characterizes the density of the medium, ω is the wave number, and u is the spatially varying pressure field arising from a disturbance at a source located at $x_s \in \Omega$. We impose the absorbing boundary condition

$$a\nabla u \cdot n - iku = 0 \quad \text{on } \partial\Omega, \tag{5.4.4}$$

where $k = a^{-1/2}\omega$. The seismic data is represented as the collections of solutions measured on the sensor domain, $\mathcal{G}(u, \nabla u, x) = u|_D$ for a set of frequencies ω.

In the numerical simulation, the parameters used are $\epsilon = 1/80, H = 1/30, h = 1/256$, and wavelengths $\omega \in \{\pi, 2\pi, 4\pi\}$. The Dirichlet data is measured on $D = \{(x_1, x_2) \mid x_1 = 0, 2; \quad x_2 \in [0,2]\}$. The following is a summary of the errors in microscale inversion of the effective model corresponding to (5.4.3).

Table 5.4 demonstrates the performance of microscale inversion of the multiscale Helmholtz equation using macroscale forward solvers. For $N = 1$, all

Table 5.4: Error in parameter inversion of the multiscale Helmholtz equation.

A. Volume fraction

N	Analytic	HMM	Two-stage
1	0.05096522	0.06306604	0.03395456
2	0.07285428	0.04647223	0.23170495
3	0.07228700	0.05222681	0.36715450
4	0.17000688	0.18484829	0.33137285
5	0.39147898	0.36494049	0.35403502
6	0.25308301	0.23206174	0.4569

B. Amplitude

N	Analytic	HMM	Two-stage
1	0.02164183	0.02564728	0.53395456
2	0.08266182	0.06451603	0.71182211
3	0.14964111	0.15981872	0.77197283
4	0.26047966	0.25863550	1.08147624
5	0.46285118	0.44164636	0.81757732
6	0.50891196	0.50168049	1.36508948

C. Angle

N	Analytic	HMM	Two-stage
1	0.06595855	0.01329244	0.00491449
2	0.16913028	0.11690812	0.21323509
3	0.78174458	0.29604107	0.38340192
4	0.48785718	0.47404862	0.37318240
5	0.43459516	0.38184943	0.53843215
6	0.75404888	0.64028093	0.35335906

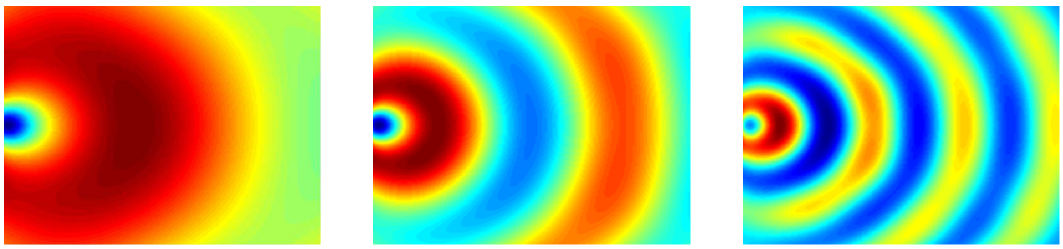

Figure 5.4: **Solutions to the multiscale Helmholtz equation.** Real part of solutions to the multiscale Helmholtz equation (5.4.3) for frequencies $\omega = \pi$, $\omega = 2\pi$, $\omega = 4\pi$ (left to right) and $a = a^{\epsilon}$ in (5.2.10).

three solvers performed well. The modeled data included high frequency solutions relative to the size of the coarse mesh; this resulted in poor performance of all of the methods for N large.

Remark 5.4.2. These techniques can be applied to the recovery of a material parameters with more general decompositions. In 5.5, the parameter m is represented using a spline basis decomposition.

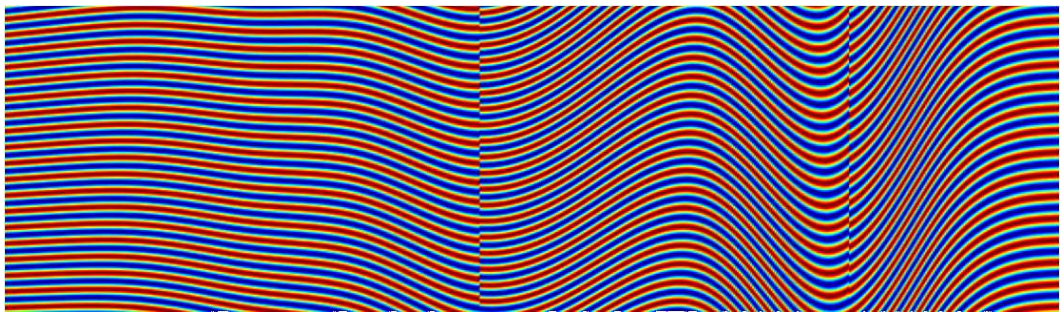

Figure 5.5: **Layered media example.** Splines are used to model the angle, amplitude, and thickness of the layers. The discontinuities can be used to model faults in earths subsurface.

Chapter 6

Conclusions

Multiscale computations aim at designing numerical algorithms for the simulation of coupled models on different scales. In the theory of homogenization of differential equations, multiscale processes are described by the combination of models on different scales. The relevant functions in the homogenization of differential equations and in the theory of heterogeneous multiscale methods (HMM) satisfy the scaling law $f^{\epsilon}(x) = f(x, x/\epsilon)$, where $f(x, y)$ is periodic in y and the parameter $0 < \epsilon << 1$ represents the ratio of scales in the problem.

We view these functions in the setting of information theory by making the further assumption that $f(x, y)$ belongs to the class of bandlimited functions in x and y and thus has a Fourier decomposition

$$f(x, y) = \sum_{k=0}^{K} f_k(x) e^{2\pi i k y}.$$

A numerical method containing both the macro and micro scales needs to deal with the effective solution on a macroscale grid of size Δx and direct numerical simulation of the oscillatory problem on smaller, local fine scale grids with spacing $\delta x < \Delta x$. We prove that a computational grid X designed to fully

resolve f^ϵ can be of the form

$$X = \{j\Delta x + k\delta x \mid j \in \mathbb{Z}, 0 \leq k \leq K\},$$

which matches sampling strategies used in information theory when applied to bandlimited signals.

The so called type A problem in HMM is also discussed. The microscale is here only relevant in one or a few locations. For these problems, there is a close connection between mesh refinement and information theory.

We also presented theoretical and numerical techniques for solving inverse problems corresponding to multiscale partial differential equations of the form

$$-\nabla \cdot (a^\epsilon \nabla u^\epsilon) + b^\epsilon u^\epsilon = f,$$

where $0 < \epsilon \ll 1$ and a^ϵ, b^ϵ are coefficients that oscillate on the ϵ—scale. Such inverse problems are often reduced to well-posed problems through the use of effective forward models by standard averaging and homogenization techniques. Obtaining these models can result in the loss of microscale information.

In our approach, we use effective forward models to make predictions and then constrain the search space to a low dimensional parameter space $m \in \mathbb{R}^N$ based on prior knowledge of the structure of the microscale. We use generic optimization routines in this proof of concept but for higher dimensional m, other minimization techniques must be used, as for example, adjoint-state based methods in geophysical applications [73].

The main theoretical contribution is a proof that in cases where the mapping $m \to a^\epsilon(m)$ is sufficiently monotone, the Dirichlet-to-Neumann map corresponding to the effective equation results in a unique recovery of a^ϵ. We provided numerical justification that indicates that multiscale methods such as HMM can be used to make forward predictions that prove useful in these microscale recovery problems, even when the explicit form of the effective equation is not known.

We also provide numerical results that demonstrate the performance of these techniques in scientific applications. If the absorption term b^ϵ is replaced with a positive, slowly varying function σ, the resulting equation is a standard model used in quantitative photoacoustic tomography (qPAT), a technique used in medical imaging [11]. If instead b^ϵ replaced by a frequency term $-\omega^2$, we have the multiscale Helmholtz equation used in seismic forward modeling.

In this dissertation, we applied the HMM philosophy to recover the parameter m from the microstructure constraint for the diffusion term, $m \to a^\epsilon(m)$, given effective solution data that mimics the physical experiments. In future research, we will consider a microscale parametrization using different basis functions, such as wavelets, and moving toward using more realistic datasets that will allow further validation of these methods. It will also be interesting to study the stochastic effect of noise.

We are also interested in developing the HMM algorithm by designing methods that adapt to prior microstructure knowledge. In [29], Du and Ming prove error estimates for the finite element heterogeneous multiscale method

for elliptic problems with nonsmooth microstructures. In order to calculate the effective coefficients, a new estimate of the corrector arising from periodic and Neumann cell problems is given. This raises the question of how to design a method for microscale models of the form $a(x, \sigma(x)x/\epsilon)$, where the cell geometry depends on a transformation matrix σ. The effects of cell geometry are not well understood, and future research will probe the effects of σ on bounds of the error induced by HMM.

Chapter 7

Bibliography

[1] A. Abdulle, W. E, B. Engquist, and E. Vanden-Eijnden. The heterogeneous multiscale method. *Acta Numerica*, 21:1–87, Apr. 2012.

[2] G. Alessandrini. Open issues of stability for the Inverse Conductivity Problem. *Journal Inverse Ill-Posed Problems*, 15(2006014115):1–10, 2007.

[3] G. Alessandrini and R. Gaburro. Determining conductivity with special anisotropy by boundary measurements. *SIAM Journal on Mathematical Analysis*, 33(1):153–171, 2001.

[4] G. Allaire. Homogenization and two-scale convergence. *SIAM Journal on Mathematical Analysis*, 1992.

[5] I. Babuška. Solution of problems with interfaces and singularities. Technical report, 1974.

[6] I. Babuška. Solution of interface problems by homogenization. I. *SIAM Journal on Mathematical Analysis*, 7(5):603–634, 1976.

[7] I. Babuška. Solution of interface problems by homogenization. II. *SIAM Journal on Mathematical Analysis*, 7(5):635–645, 1976.

[8] I. Babuška. Solution of interface problems by homogenization. III. *SIAM Journal on Mathematical Analysis*, 8(6):923–937, 1977.

[9] G. Baeten, J. W. de Maag, R.-E. Plessix, R. Klaassen, T. Qureshi, M. Kleemeyer, F. ten Kroode, and Z. Rujie. The use of low frequencies in a full-waveform inversion and impedance inversion land seismic case study. *Geophysical Prospecting*, 61(4):701–711, July 2013.

[10] G. Bal and K. Ren. Multi-source quantitative PAT in diffusive regime. *Inverse Problems*, 27:1–24, 2011.

[11] G. Bal and K. Ren. On multi-spectral quantitative photoacoustic tomography in diffusive regime. *Inverse Problems*, 28(2):025010, Feb. 2012.

[12] H. Behmard and A. Faridani. Sampling of bandlimited functions on unions of shifted lattices. *Journal of Fourier Analysis and Applications*, pages 1–22, 2002.

[13] J. J. Benedetto and P. J. S. G. Ferreira, editors. *Modern Sampling Theory*. Birkhäuser Boston, Boston, MA, 2001.

[14] J. J. Benedetto and W. Heller. Irregular sampling and the theory of frames, I, Jan. 1990.

[15] A. Bensoussan, J. L. Lions, and G. Papanicolaou. *Asymptotic Analysis for Periodic Structures*, volume 5 of *Studies in Mathematics and its Applications*. North-Holland Pub. Co. (Amsterdam and New York and New York), 1978.

[16] A. Beurling and L. Carleston. *The Collected works of Arne Beurling*. Birkhauser, Boston, MA, 1989.

[17] L. Borcea. Electrical impedance tomography. *Inverse Problems*, 18(6):R99–R136, Dec. 2002.

[18] A. Braides. *Gamma-convergence for Beginners*, volume 22. Oxford University Press, 2002.

[19] A. P. Calderón. On an inverse boundary value problem. *Computational & Applied Mathematics*, 25(2-3):133–138, 2006.

[20] J. Cartwright. The impact of 3D seismic data on the understanding of compaction, fluid flow and diagenesis in sedimentary basins. *Journal of the Geological Society*, 164(5):881–893, 2007.

[21] A. Cauchy. Mémoire sur diverses formules d'analyze. *Comptes Rendus des Séances de l'Académie des Sciences*, 12(6):183–298, 1841.

[22] M. Cheney, D. Isaacson, and J. C. Newell. Electrical Impedance Tomography. *SIAM Review*, 41(1):85–101, Jan. 1999.

[23] D. Cioranescu and P. Donato. *An introduction to homogenization*. 1999.

[24] J. J. Clark, M. R. Palmer, and P. D. Lawrence. A transformation method for the reconstruction of functions from nonuniformly spaced samples. *IEEE Transactions on Acoustics, Speech, and Signal Processing*, 33(5):1151–1165, Oct. 1985.

[25] G. Dal Maso. *An introduction to G-convergence*. Springer, 1993.

[26] E. De Giorgi and G. Dal Maso. Γ-Convergence and calculus of variations. In *Mathematical theories of optimization*, pages 121–143. Springer, 1983.

[27] E. De Giorgi and T. Franzoni. Su un tipo di convergenza variazionale. *Atti Accad. Naz. Lincei Rend. Cl. Sci. Fis. Mat. Natur.(8)*, 58(6):842–850, 1975.

[28] M. Desbrun, R. Donaldson, and H. Owhadi. Discrete geometric structures in homogenization and inverse homogenization with application to EIT. *arXiv preprint arXiv:0904.2601*, 2009.

[29] R. Du and P. Ming. Convergence of the heterogeneous multiscale finite element method for elliptic problems with nonsmooth microstructures. *Multiscale Modeling & Simulation*, 8(5):1770–1783, 2010.

[30] R. J. Duffin and A. C. Schaeffer. A Class of Nonharmonic Fourier Series. *Transactions of the American Mathematical Society*, 72(2):341 – 366, 1952.

[31] W. E. *Principles of Multiscale Modeling*. Cambridge University Press, 2011.

[32] W. E and B. Engquist. The heterogenous multiscale methods. *Communications in Mathematical Sciences*, 1(1):87–132, Mar. 2003.

[33] Y. Efendiev and T. Y. Hou. *Multiscale finite element methods: theory and applications*, volume 4. Springer, 2009.

[34] B. Engquist. Multi-scale Modeling. In S. Benedicks, Michael and Jones, Peter W. and Smirnov and W. Björn, editors, *Perspectives in Analysis*, volume 27 of *Mathematical Physics Studies*, pages 51–63. Springer Berlin Heidelberg, 2005.

[35] B. Engquist, X. Li, W. Ren, E. Vanden-Eijnden, and W. E. Heterogeneous multiscale methods: a review. *Commun. Comput. Phys.*, 2(3):367–450, 2007.

[36] B. Engquist and Y.-H. Tsai. Heterogeneous multiscale methods for stiff ordinary differential equations. *Mathematics of Computation*, 74(252):1707–1742, 2005.

[37] L. C. Evans. *Partial Differential Equations*, volume 19. 1998.

[38] H. Feichtinger and K. Gröchenig. Theory and practice of irregular sampling. *Wavelets: mathematics and applications*, pages 1–56, 1994.

[39] H. Feichtinger, K. Gröchenig, and T. Strohmer. Efficient numerical methods in non-uniform sampling theory. *Numerische Mathematik*, 1995.

[40] H. G. Feichtinger and K. Gröchenig. Iterative reconstruction of multivariate band-limited functions from irregular sampling values. *SIAM Journal on Mathematical Analysis*, 23(1):244–261, Jan. 1992.

[41] A. Fichtner, J. Trampert, P. Cupillard, E. Saygin, T. Taymaz, Y. Capdeville, and A. Villasenor. Multiscale full waveform inversion. *Geophysical Journal International*, 194(1):534–556, Apr. 2013.

[42] J. Fish, V. Filonova, and S. Kuznetsov. Micro-inertia effects in nonlinear heterogeneous media. *International Journal for Numerical Methods in Engineering*, 91(13):1406–1426, Sept. 2012.

[43] C. W. Freudiger, W. Min, B. G. Saar, S. Lu, G. R. Holtom, C. He, J. C. Tsai, J. X. Kang, and X. S. Xie. Label-free biomedical imaging with high sensitivity by stimulated Raman scattering microscopy. *Science (New York, N.Y.)*, 322(5909):1857–61, Dec. 2008.

[44] B. Ganapathysubramanian and N. Zabaras. Modeling diffusion in random heterogeneous media: Data-driven models, stochastic collocation and the variational multiscale method. *Journal of Computational Physics*, 226(1):326–353, Sept. 2007.

[45] W. Gautschi. How (Un) stable are Vandermonde systems? *Asymptotic and computational analysis*, pages 193–210, 1990.

[46] K. Gröchenig. Reconstruction algorithms in irregular sampling. *Mathematics of Computation*, 1992.

[47] K. Gröchenig and T. Strohmer. Numerical and theoretical aspects of nonuniform sampling of band-limited images. *Nonuniform Sampling*, 2001.

[48] T. Y. Hou and X.-H. Wu. A multiscale finite element method for elliptic problems in composite materials and porous media. *Journal of computational physics*, 134(1):169–189, 1997.

[49] F. Ihlenburg and I. Babuška. Solution of Helmholtz problems by knowledge-based FEM. *Computer Assisted Mechanics and Engineering Sciences*, (2):397–415, 1997.

[50] A. Jerri. The Shannon sampling theorem-Its various extensions and applications: A tutorial review. *Proceedings of the IEEE*, 65(11):1565–1596, 1977.

[51] V. V. Jikov, S. M. Kozlov, and O. A. Oleinik. *Homogenization of Differential Operators and Integral Functionals*. Springer, 2011.

[52] A. Kempf. Filtering, Sampling, and Reconstruction With Time-Varying Bandwidths. *IEEE Signal Processing Letters*, 17(3):241–244, Mar. 2010.

[53] I. Kluvánek. Sampling theorem in abstract harmonic analysis. *Matematicko-fyzikálny časopis*, 1965.

[54] A. Kohlenberg. Exact Interpolation of Band-Limited Functions. *Journal of Applied Physics*, 24(12):1432, 1953.

[55] V. Kotel'nikov. On the carrying capacity of the ether and wire in telecommunications. *Material for the First All-Union Conference on Questions of Communication*, 1933.

[56] B. Kouchmeshky and N. Zabaras. The effect of multiple sources of uncertainty on the convex hull of material properties of polycrystals. *Computational Materials Science*, 47(2):342–352, Dec. 2009.

[57] H. J. Landau. Necessary density conditions for sampling and interpolation of certain entire functions. *Acta Mathematica*, 117(1):37–52, July 1967.

[58] H. J. Landau. Sampling, data transmission, and the Nyquist rate. *Proceedings of the IEEE*, 55(10):1701–1706, Oct. 1967.

[59] E. Margolis and Y. C. Eldar. Nonuniform Sampling of Periodic Bandlimited Signals. *IEEE Transactions on Signal Processing*, 56(7):2728–2745, 2008.

[60] R. J. Marks. Ill-posed sampling theorems. *IEEE Transactions on Circuits and Systems*, 32(5):481–484, May 1985.

[61] R. J. Marks. *Advanced topics in Shannon Sampling and Interpolation Theory*. Springer Texts in Electrical Engineering. Springer-Verlag, 1993.

[62] F. A. Marvasti. *Nonuniform sampling*. Kluwer Academic/Plenum Publishers, 2001.

[63] P. Ming and P. Zhang. Analysis of the heterogeneous multiscale method for elliptic homogenization problems. *Journal of the American Mathematical Society*, 18(1):121–156, 2005.

[64] W. Mulder and R.-E. Plessix. Exploring some issues in acoustic full waveform inversion. *Geophysical Prospecting*, 56(6):827–841, Nov. 2008.

[65] F. Murat and L. Tartar. H-convergence,"Séminaire d'Analyse Fonctionnelle et Numérique de l'Université d'Alger", mimeographed notes, 1978. English translation in Topics in the mathematical modelling of composite materials

(A. Cherkaev and R. Kohn, Eds.). *Progress in Nonlinear Differential Equations and their Applications*, 31, 1994.

[66] H. Nyquist. Certain Topics in Telegraph Transmission Theory. *Transactions of the American Institute of Electrical Engineers*, 47(2):617–644, Apr. 1928.

[67] A. Papoulis. Generalized sampling expansion. *IEEE Transactions on Circuits and Systems*, 24(11):652–654, Nov. 1977.

[68] A. Papoulis. *Signal analysis*. McGraw-Hill, 1977.

[69] G. Pavliotis and A. Stuart. *Multiscale Methods: Averaging and Homogenization*, volume 53. Springer, 2008.

[70] G. Pavliotis, A. Stuart, and J. Nolen. Multiscale modelling and inverse problems. In I. G. Graham, T. Y. Hou, O. Lakkis, and R. Scheichl, editors, *Numerical Analysis of Multiscale Problems*, pages 1–34. Springer Berlin Heidelberg, 2012.

[71] D. P. Petersen and D. Middleton. Sampling and reconstruction of wave-number-limited functions in N-dimensional Euclidean spaces. *Information and Control*, 5(4):279–323, Dec. 1962.

[72] M. A. Pinsky. *Introduction to Fourier Analysis and Wavelets*. American Mathematical Society, 2002.

[73] R.-E. Plessix. A review of the adjoint-state method for computing the gradient of a functional with geophysical applications. *Geophysical Journal International*, 167(2):495–503, Nov. 2006.

[74] R. S. Prendergast, B. C. Levy, and P. J. Hurst. Reconstruction of Bandlimited Periodic Nonuniformly Sampled Signals through Multirate Filter Banks. *IEEE Transactions on Circuits and Systems I: Regular Papers*, 51(8):1–11, 2004.

[75] M. Ptashnyk. Two-scale convergence for locally periodic microstructures and homogenization of plywood structures. *Multiscale Modeling & Simulation*, 11(1):92–117, 2013.

[76] C. E. Shannon. Communication in the presence of noise. *Proceedings of the IRE*, 37(1):10–21, Feb. 1949.

[77] C. E. Shannon and W. Weaver. The Mathematical Theory of Communication. *MD computing computers in medical practice*, 14(4):306–17, 1948.

[78] L. Sirgue and R. G. Pratt. Efficient waveform inversion and imaging: A strategy for selecting temporal frequencies. *Geophysics*, 69(1):231–248, Jan. 2004.

[79] S. Spagnolo. Sulla convergenza di soluzioni di equazioni paraboliche ed ellittiche. *Annali della Scuola Normale Superiore di Pisa-Classe di Scienze*, 22(4):571–597, 1968.

[80] S. Spagnolo. Convergence in energy for elliptic operators. *Numerical Solutions of Partial Differential Equations III, Acad. Press, New York*, 1976.

[81] T. Strohmer. Computationally attractive reconstruction of bandlimited images from irregular samples. *IEEE transactions on image processing : a publication of the IEEE Signal Processing Society*, 6(4):540–8, Jan. 1997.

[82] W. W. Symes. The seismic reflection inverse problem. *Inverse Problems*, 25(12), Dec. 2009.

[83] L. Tartar. Problemes de contrôle des coefficients dans des équations aux dérivées partielles. In *Control Theory, Numerical Methods and Computer Systems Modelling*, pages 420–426. Springer, 1975.

[84] G. Uhlmann. The Dirichlet to Neumann Map and Inverse Problems. Technical report.

[85] G. Uhlmann. Commentary on Calderón's paper 28 , On an Inverse Boundary Value Problem. *Selected papers of Alberto P. Calderón*, pages 1–12, 2008.

[86] M. Unser. Sampling-50 years after Shannon. *Proceedings of the IEEE*, 88(4):569–587, 2000.

[87] P. P. Vaidyanathan. Periodically nonuniform sampling of bandpass signals. *IEEE Transactions on Circuits and Systems II: Analog and Digital Signal Processing*, 45(3):340–351, Mar. 1998.

[88] P. P. Vaidyanathan. Generalizations of the sampling theorem: Seven decades after Nyquist. *Circuits and Systems I: Fundamental Theory and applications*, 48(9):1094–1109, 2001.

[89] R. Venkataramani and Y. Bresler. Perfect reconstruction formulas and bounds on aliasing error in sub-Nyquist nonuniform sampling of multiband signals. *IEEE Transactions on Information Theory*, 46(6):2173–2183, 2000.

[90] R. Venkataramani and Y. Bresler. Sampling theorems for uniform and periodic nonuniform mimo sampling of multiband signals. *IEEE Transactions on Signal Processing*, 51(12):3152–3163, Dec. 2003.

[91] E. Whittaker. On the functions which are represented by the expansion of the interpolation theory. *Proceedings of the Edinburgh Mathematical Society*, 35(Sect. A):181–194, 1915.

[92] J. M. Whittaker. On the Cardinal Function of Interpolation Theory. *Proceedings of the Edinburgh Mathematical Society*, 1(2):41–46, Jan. 1927.

[93] J. M. Whittaker. *Interpolatory function theory*. Cambridge University Press, Cambridge, 1935.

[94] R. Wiley. Recovery of Bandlimited Signals from Unequally Spaced Samples. *IEEE Transactions on Communications*, 26(1):135–137, Jan. 1978.

[95] J. Yen. On Nonuniform Sampling of Bandwidth-Limited Signals. *IRE Transactions on Circuit Theory*, 3(4):251–257, 1956.

[96] X. Yue. The local microscale problem in the multiscale modeling of strongly heterogeneous media: Effects of boundary conditions and cell size. *Journal of Computational Physics*, 222(2):556–572, Mar. 2007.